Mon. Not. R. astr. Soc. (1986) **220,** 19–49

Refractive effects in pulsar scintillation

Roger W. Romani, Ramesh Narayan and Roger Blandford *Theoretical Astrophysics, California Institute of Technology, Pasadena, CA 91125, USA*

Accepted 1985 October 24. Received 1985 October 14; in original form 1985 May 13

Summary. Recent studies have focused attention on the refractive effects of long-wavelength ($\lesssim 10^{14}$ cm) electron density fluctuations in the interstellar medium upon radio observations of pulsars and compact extragalactic radio sources. In earlier work, a simple scattering model was introduced which allowed us to compute fluctuations in mean intensity, image size, pulse width and pulse arrival time, along with their cross-correlations and fluctuation time-scales, when there is a power-law spectrum of density perturbations in a thin 'equivalent screen' of scattering material. In this work, we extend the analysis to include refraction-induced fluctuations in intrinsically diffractive quantities such as the scintillation time-scale, t_s, and the decorrelation bandwidth, ν_{dc}. We then use the theory to study the drifting bands in dynamic scintillation spectra caused by the dispersive steering of the diffraction pattern. We also estimate the fluctuations in the position of the image on the sky, rates of variation of intensity and position, and the root mean square elongation of the scatter-broadened image. We make two further extensions of the theory. First we show that, despite certain formal divergences, the theory can be extended to accommodate steeper density fluctuation spectra (power-law indices $\beta > 4$) than the conventionally assumed Kolmogorov spectrum ($\beta = 11/3$). Secondly, we test the validity of the thin-screen approximation, developing a formalism to treat scattering in an extended medium. We find that the thin-screen theory sometimes underestimates the refractive fluctuations by a factor ~ 2. The auto- and cross-correlations of the various observables are calculated and comparison is made with the known scintillation properties of pulsars to select those effects most suited to observational verification. The predicted cross-correlation between decorrelation bandwidth and flux fluctuations seems particularly suitable for this purpose. These measurements should, in turn, provide insights into the density fluctuation spectrum and the distribution of the scattering along the line-of-sight.

1 Introduction

The effect of small-scale electron density perturbations in the interstellar medium upon the propagation of pulsar radio signals has been recognized since the earliest observations (Scheuer 1968; Rickett 1977; Manchester & Taylor 1977). These inhomogeneities scatter the rays by a root mean square scattering angle θ in propagating a distance D to Earth. The extra path-length traversed by a given ray leads to a mean time delay $t \sim D\theta^2/2c$ and the dispersion in this value among a large number of received rays causes a *pulse broadening* of the same magnitude. Since the phases of the independent rays are essentially uncorrelated, they can interfere to produce deep scintillation, and this creates a diffraction pattern at Earth with a lateral coherence length $b \sim \lambda/2\pi\theta$. The motion of an observer relative to this pattern at a speed v, dominated by the pulsar's peculiar velocity, leads to a diffractive *scintillation time-scale*, $t_s \sim b/v$, and a *decorrelation bandwidth*, $\nu_{dc} \sim c/\pi D\theta^2$.

It has been argued on observational grounds (e.g. Lee & Jokipii 1975; Rickett 1977) that the electron density perturbations have a three-dimensional power spectrum in the form of a power law, $\Phi_k \propto k^{-\beta}$, $2<\beta<4$, i.e. the density fluctuations on a scale a vary as $\delta n(a) \propto a^{(\beta-3)/2}$. The scattering angle induced in scale a is $\delta\eta \sim \delta n(a)\, r_e \lambda^2/2\pi$, where $r_e = e^2/mc^2$. If there are D/a such regions along the pulsar–Earth path then the scatterings will add incoherently to give an rms scattering angle $\theta(a) \sim (D/a)^{1/2}\delta\eta \sim a^{(\beta-4)/2}\lambda^2 D^{1/2}$. Hence, for $\beta<4$, the scattering will be dominated by the smallest scale a_{min} (the 'diffractive' scale) for which phase fluctuations satisfy $\phi(a_{min}) \sim a_{min}\theta/\lambda > \pi$, the strong scattering condition. Provided $a_{min} < \theta D$ (the multi-path condition), as is true for interstellar scintillation, the angular size of the image scales as $\theta \propto \lambda^{\beta/(\beta-2)} D^{1/(\beta-2)}$. Observations reveal that $\partial(\log\theta)/\partial(\log\lambda) \gtrsim 2$ (e.g. Mutel *et al.* 1974), implying that β is close to the critical value 4. Kolmogorov turbulence theory predicts that

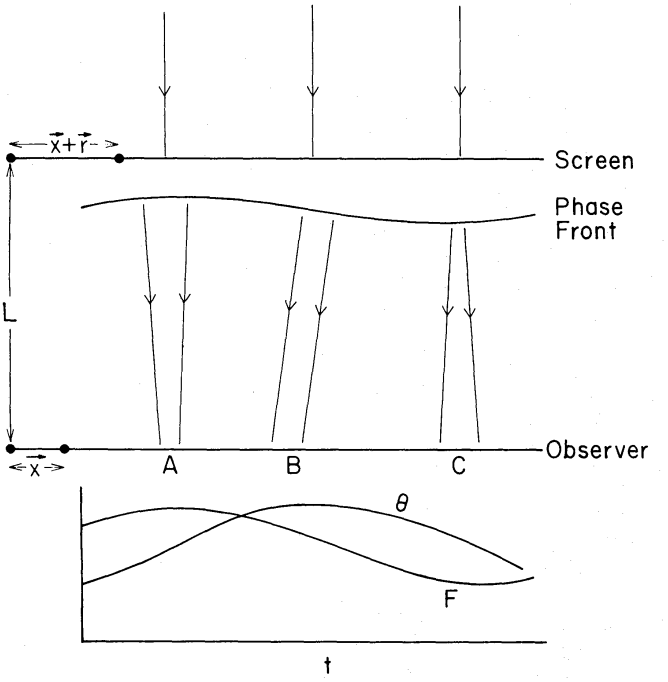

Figure 1. Schematic representation of the focusing and steering effects of refractive perturbations. The upper section shows the effect of an incident plane wave of a thin screen with a single long-wavelength sine-wave perturbation. As the observer moves relative to the resulting intensity distribution, the flux F and position of the source θ are modulated as shown below. F is maximal at A, varies most rapidly at B and is minimal at C. Thus F correlates with the rate of change of θ and vice-versa.

$\beta=11/3$, and it has been argued that the observational data are consistent with this value (Lee & Jokipii 1975; Armstrong, Cordes & Rickett 1981).

Recently, there has been increasing evidence that perturbations much larger than the diffractive scale $a_{\min}$ are also important in the propagation of radio waves in the interstellar medium. In particular, it seems that electron density perturbations on a scale comparable to the size of the scatter-broadened spot on the sky, $\sigma\sim\theta D$ (the 'refractive' scale), can cause refractive focusing and defocusing of the pulsar image (see Fig. 1) on a time-scale $\sim T_{\rm ref}=\sigma/v$. Rickett, Coles & Bourgois (1984), following Sieber (1982) (*cf.* also Shapirovskaya 1978), proposed that these effects may account for long period (~days–years) variations in pulsar intensity as well as the low-frequency variability of compact extragalactic radio sources. In addition, the sloping drift patterns of pulsar dynamic scintillation spectra could also arise from the influence of these large scales (Shishov 1974; Hewish 1980; Roberts & Ables 1982; Hewish, Wolszczan & Graham 1985).

Blandford & Narayan (1984), pointed out that, in addition to the received flux, many other observed parameters, such as angular size and pulse width, can also vary due to refractive perturbations. In a later paper (Blandford & Narayan 1985, hereafter BN), they developed a simple model based on the thin-screen approximation (reviewed in Section 2), to calculate the magnitudes of the various fluctuations and the correlations among them. In this model, it is assumed that short-wavelength fluctuations on scales $\gtrsim a_{\min}$ scatter the incident radiation into an approximately Gaussian beam when averaged over an area on the screen with dimensions $\gg a_{\min}$, but $\ll\sigma$. Equivalently, an observer sees a Gaussian image provided the observations are averaged over a time $t_{\rm a}$ such that $t_{\rm s}\ll t_{\rm a}\ll T_{\rm ref}$. The long-wavelength 'refractive' fluctuations on scales $\sim\sigma$ are then modelled as introducing a smooth large-scale slope and curvature to the phase front, which are responsible for steering and focusing the independent Gaussian beams emerging from the screen. The theory then goes on to assume that the refractive bending is small compared to that due to the small scales and so linearizes the problem. This is an approximate model and there would be no need for it if we were interested only in intensity fluctuations, since more powerful and exact techniques have been developed for that purpose (e.g. Salpeter 1967; Gochelashvily & Shishov 1975; Rumsey 1975; Prokhorov *et al.* 1975; Uscinski 1977; Rino 1979; Tatarskii & Zavorotnyi 1980; Jakeman 1982; Goodman & Narayan 1985, hereafter GN, as representatives of an extensive literature). However, in BN as well as the present paper, we are most interested in giving a semi-quantitative discussion of fluctuations in *other potentially observable quantities* for which we cannot perform accurate calculations, and this necessitates using our model. Nevertheless we have used the above-quoted more accurate intensity fluctuation computations to verify that our approximations are quite accurate (see Appendix C). We also show in Appendix B that our two-scale approach can be motivated starting from a more formal theory. The discussion there, as well as the qualitative argument given above, indicate that our approximations are most accurate when the diffractive and refractive scales are well separated. This is equivalent to requiring very strong scintillation [i.e. rms phase fluctuations in the Fresnel scale, $\phi(\sqrt{\lambda D})\gg1$], which is fortunately the case in the interstellar medium at low radio frequencies.

There is a second feature of our model that deserves comment and this concerns the importance of caustics. As we are concerned with strong scintillation from phase-thick screens, geometrical optics is a valid description of the scattering due to refractive scales. If the diffractive scales were missing altogether and if the rms curvature in the phase fluctuations were such as to bring rays to a focus at the observer distance D, then the observed intensity record would display a series of sharp spikes as the observer moved through successive *caustic* surfaces. Our theory, which limits itself to the lowest order in a perturbative expansion of refractive effects, would be quite inadequate to handle this situation. However, our primary interest in this paper is in an extended power-law phase fluctuations spectrum $\phi(k)\propto k^{-\beta}$ with $\beta<4$. in this case, since the scattering angle on scale a goes as $\theta(a)\propto a^{(\beta-4)/2}$, the typical focal length of fluctuations on the

refractive scale σ is $\sim D(\sigma/a_{\min})^{(\beta-4)/2} \gg D$. Thus we are justified in quantifying the refractive effects through a linear approximation. Phase fluctuations on scales smaller than σ do have sufficient curvature to focus at the observer, but they do not produce sharp spikes in the intensity record because of the presence of the other length-scales (*cf.* Salpeter 1967).

The technique employed in BN and in this paper involves *intensity*-weighted averages of quantities of interest. A simple extension of the BN analysis allows us to estimate in Section 2 the fluctuations in the observed source position, which is of interest for VLBI observations of radio sources. The jitter in the source position should be correlated with fluctuations in $\dot{F}$ (the rate of variation of flux F) as shown in Fig. 1. We also consider the random elongation of the scatter-broadened image.

At first sight it might appear that an intensity-weighted approach such as ours would be quite unsuitable for a description of diffraction-related phenomena like the decorrelation bandwidth $\nu_{\rm dc}$ or the scintillation time-scale $t_{\rm s}$. In actual fact, as we show in Section 3, the theory is capable of treating these phenomena as well. Since $\nu_{\rm dc}$ and $t_{\rm s}$ are related to the angular spread in the rays received, their fluctuations are correlated with variations in the flux, angular size Ω, pulse broadening τ, etc. Another interesting diffractive phenomenon that we study is the drifting bands seen in dynamic scintillation spectra. The sloping patterns are believed to be produced by gradients or 'prisms' in the scattering medium (Shishov 1974; Hewish 1980); they should thus be correlated with position shifts and $\dot{F}$. In Section 4 we evaluate the correlations among the various observables for power-law spectra of density perturbations.

As mentioned above, the analysis used in BN and in this paper requires that the scattering due to refractive scales be smaller than the small-scale scattering, θ. This is valid in the strong scintillation regime provided the spectral exponent $\beta \leqq 4$. Recently, however, there has been some suggestion that β may exceed 4 (BN, GN, Hewish *et al.* 1985). We show in Section 5 that, although the refractive scattering angle can in principle diverge for $\beta > 4$, a simple ('renormalization' of the theory enables us to handle even this regime to some extent. Another important question concerns the validity of the thin-screen approximation when the scattering probably occurs in several screens or an extended medium. We consider this issue in Section 6 using an extension of our formalism and find that a single screen underestimates the magnitude of refractive flux fluctuations by a factor of ~ 2.

In Section 7 we give numerical estimates of the various fluctuations for power-law spectra with $\beta = 11/3$, 4 and 4.3. The magnitudes of the observable quantities as well as their scalings as a function of λ, D, velocity v, and the strength of the density perturbations C_N^2 are collected together in Table 1. The magnitudes of the cross-correlations are presented in Table 2 and the relevant formulae are given in Appendix A. Using these, we discuss in Section 8 the feasibility of detecting the various refractive effects. Refractive fluctuations in diffractive quantities such as $t_{\rm s}$ and $\nu_{\rm dc}$ seem to be quite suitable for experimental verification, particularly since the measurements can be made at short radio wavelengths, where the refractive time-scale $T_{\rm ref} \sim D\theta/v$ is short. We urge that such observations be carried out in order to confirm that refractive scintillation effects do occur in the interstellar medium.

A point to note is that the slopes of drifting bands in dynamic scintillation spectra are sensitive to density fluctuations on scales much larger than the refractive scale σ. Hence they are particularly well-suited to placing limits on the outer scale $r_{\rm out}$ (i.e. large length scale cut-off) of the density fluctuation spectrum. The data on drift slopes presently available seem already to suggest that an outer scale must be present and that a simple power-law model of the fluctuation spectrum may be too simplistic. An outer scale is also suggested in several cases by the physical requirement that the electron density fluctuation $\delta n(a)$ on a scale a must not exceed the mean density n. This places stringent limits on $r_{\rm out}$ in regions of high C_N^2, such as the lines-of-sight to the Vela pulsar and the centre of our Galaxy.

Table 1. Numerical estimates and scalings of scintillation parameters for power-law spectra of interstellar electron density fluctuation with $\beta=11/3$, 4 and 4.3. D is in kpc, λ in m, $C_{-4}=10^4 C_N^2$ (C_N^2 as in Armstrong *et al.* 1984) and γ is defined in equation (7.4). The increase in amplitude of the refractive fluctuations with increasing β is explicitly seen. An asterisk (*) denotes an estimate for the fluctuations about the measured mean (e.g. 5.5) over an observation period T_y in years. v_7 is the combined Earth–pulsar velocity in 10^7 cm s^{-1}; the equivalent spatial lag of the observation period is written $s=v_7 T_y$.

$$\mu=\ln\left(\frac{v_7 T_y}{\gamma^{0.5} C_{-4}^{0.5}\lambda^2 D^{1.5}}\right)$$

is a logarithmic correction factor for θ_x and $\beta=4$. For $\beta\geq 4$, e_d and m_d depend strongly on the outer scale and are therefore omitted.

	$\beta=11/3$	$\beta=4$	$\beta=4.3$
θ (mas)	$2.2C_{-4}^{0.6}\lambda^{2.2}D^{0.6}$	$2.2\gamma^{0.5}C_{-4}^{0.5}\lambda^2 D^{0.5}$	$2.2C_{-4}^{0.59}\lambda^{2.4}D^{0.76}$
τ (μs)	$2.9C_{0.4}^{1.2}\lambda^{4.4}D^{2.2}$	$2.9\gamma C_{-4}^{1.0}\lambda^4 D^2$	$2.9C_{-4}^{1.2}\lambda^{4.8}D^{2.5}$
ω_{dc} (kHz)	$54C_{-4}^{1.2}\lambda^{-4.4}D^{-2.2}$	$54\gamma^{-1}C_{-4}^{-1}\gamma^{-4}D^{-2}$	$54C_{-4}^{-1.2}\lambda^{-4.7}D^{-2.5}$
t_s (s)	$149C_{-4}^{-0.6}\lambda^{-1.2}D^{-0.6}v^{-1}$	$149\gamma^{-0.05}C_{-4}^{-0.5}\lambda^{-1}D^{-0.5}v_7^{-1}$	$149C_{-4}^{-0.59}\gamma^{-1.4}D^{-0.76}v_7^{-1}$
T_{ref} (D)	$19C_{-4}^{0.6}\lambda^{2.2}D^{1.6}v_7^{-1}$	$19\gamma^{0.5}C_{-4}^{0.5}\lambda^2 D^{1.5}v_7^{-1}$	$19C2_{-4}^{0.59}\lambda^{2.4}D^{1.76}v_7^{-1}$
δF	$0.12C_{-4}^{-0.2}\lambda^{-0.57}D^{-0.37}$	$0.38\gamma^{-0.5}$	0.55
$2\Delta\theta$ (mas)	$0.17C_{-4}^{0.4}\lambda^{1.6}D^{0.23}$	$0.58C^{0.5}\lambda^2 D^{0.5}$	$0.89C_{-4}^{0.59}\lambda^{2.4}D^{0.76}$
Δt (μs)	$1.2C_{-4}^{0.31}\lambda^2 D^{0.5}s^{0.83}$*	$4.3C_{-4}^{0.5}\lambda^2 D^{-0.5}s$*	$6.7C_{-4}^{0.52}\lambda^2 D^{0.5}s^{1.2}$*
$\Delta\tau$ (μs)	$0.30C_{-4}^{1.0}\lambda^{3.8}D^{1.8}$	$1.0\gamma^{0.5}C_{-4}^{1}\lambda^4 D^2$	$1.6C_{-4}^{1.2}\lambda^{4.7}D^{2.5}$
$\Delta\dot{F}$ (d^{-1})	$\left(\frac{1}{150}\right)C_{-4}^{-0.80}\lambda^{-2.8}D^{-2.0}v_7$	$\left(\frac{1}{50}\right)\gamma^{-1}C_{-4}^{-0.5}\lambda^{-2}D^{-1.5}v_7$	$\left(\frac{1}{37}\right)C_{-4}^{-0.59}\lambda^{-2.4}D^{-1.8}v_7$
$\Delta\theta_x$ (mas)	$0.32C_{-4}^{0.40}\lambda^{1.6}D^{0.23}$	$0.62\gamma^{-0.5}C_{-4}^{0.5}\lambda^2 D^{0.5}\mu$*	$1.5C_{-4}^{0.5}\lambda^{2.0}D^{0.5}s^{0.15}$*
$\Delta\dot{\theta}$ (mas/d)	$\left(\frac{1}{109}\right)C_{-4}^{-0.20}\lambda^{-0.57}D^{-1.4}v_7$	$\left(\frac{1}{45}\right)\gamma^{-0.5}D^{-1}v_7$	$\left(\frac{1}{28}\right)D^{-1}v_7$
Δv_{dc} (kHz)	$5.3C_{-4}^{-1.4}\lambda^{-5.0}D^{-2.6}$	$19\gamma^{-1.5}C_{-4}^{-1}\lambda^{-4}D^{-2}$	$31C_{-4}^{-1.2}\lambda^{-4.7}D^{-2.5}$
Δt_s (s)	$7.1C_{-4}^{-0.80}\lambda^{-1.8}D^{-0.97}v_7^{-1}$	$25\gamma^{-1}C_{-4}^{-0.5}\lambda^{-1}D^{-0.5}v_7^{-1}$	$37C_{-4}^{-0.59}\lambda^{-1.4}D^{-0.76}v_7^{-1}$
e_s	$0.08C_{-4}^{-0.20}\lambda^{-0.57}D^{-0.37}$	$0.27\gamma^{-0.5}$	0.40
e_d	$0.36C_{-4}^{-0.20}\lambda^{-0.57}D^{-0.57}$	–	–
m_d	$0.50C_{-4}^{-0.20}\lambda^{-0.57}D^{-0.37}$	–	–

2 The scattering model and refractive fluctuations

BN treated the effects of long-wavelength ('refractive') fluctuations in the ISM as weak perturbations of an underlying bundle of rays scatter-broadened by the diffractive scale inhomogeneities. When averaged over a time much greater than the scintillation time-scale t_s, the image of a point source, such as a pulsar, will be essentially Gaussian with a characteristic angular radius θ. This Gaussian bundle will be focused, defocused, steered, etc. (Fig. 1) by density fluctuations on the scale of the 'spot' or image size, σ. For simplicity, the refractive effect of the scattering medium is estimated in terms of an equivalent thin screen with large-scale phase variations, $\phi(\mathbf{r})$; the scattering strength of the screen and its distance from the observer, L, are adjusted so that the observed angular size θ of a point source as well as the mean geometrical time delay ($t=L\theta^2/2c$) are the same as in the model of the medium (see Appendix A in BN). The spot size on the screen will then be $\sigma\sim\theta L$. The extra refractive bending angle $\boldsymbol{\eta}(\mathbf{r})$ of a ray at transverse location $\mathbf{r}$ on the screen is given by

$$\boldsymbol{\eta}(\mathbf{r})=-\lambda\{\partial\phi(\mathbf{r})/\partial\mathbf{r}\}, \qquad (2.1)$$

where $\lambda=\lambda/2\pi$.

Table 2. Normalized cross-correlations as defined in equation (7.8) for power-law spectra of interstellar electron density fluctuations. Each entry consists of three values corresponding from top to bottom to $\beta=11/3$, 4 and 4.3, respectively. The flux F, angular size Ω, decorrelation bandwidth ν_{dc}, scintillation time-scale t_s and the position shift derivative $\dot{\theta}$ correlate with one another. Cross-correlations with the pulse broadening τ are identical to those with ν_{dc}, but with the opposite sign. The rate of flux variation $\dot{F}$ correlates with position shift θ_x and drift slope m_d. For $\beta \geq 4$, m_d diverges in the absence of an outer scale and therefore the corresponding correlations have been omitted.

	Ω	ν_{dc}	t_s	$\dot{\theta}$	
	0.61	−0.76	−0.50	−0.125	
	0.71	−0.80	−0.58	0.00	F
	0.78	−0.84	−0.64	0.13	
		−0.91	−0.82	0.56	
		−0.94	−0.82	0.58	Ω
		−0.96	−0.82	0.61	
	0.06		0.75	−0.37	
$\dot{F}$	0.00		0.77	−0.44	ν_{dc}
	–		0.79	−0.51	
	0.10	0.07		−0.69	
m_d	–	–		−0.71	t_s
	–	–		−0.74	
	$\delta\theta_x$	$\dot{F}$			

Since the diffraction pattern is moving relative to the observer (due to the motions of the pulsar, Earth and the medium), the time dependence of the various observable quantities will be given by their spatial dependence in the observer plane (see Fig. 1). Thus if $\bar{F}$ is the mean flux from the source, then the intensity received at a general point $\mathbf{x}$ from unit area around the point $\mathbf{x}+\mathbf{r}$ on the screen is

$$I(\mathbf{r},\mathbf{x})=\frac{\bar{F}}{\pi\sigma^2}\exp\left\{-\left(\frac{L\boldsymbol{\eta}+\mathbf{r}}{\sigma}\right)^2\right\}, \tag{2.2}$$

where η is evaluated at the point $(\mathbf{x}+\mathbf{r})$ and we have assumed a Gaussian spot shape. A more formal justification of this approximation is given in Appendix B. As the deflection η is, by assumption, small compared with σ/L, we can expand the argument of the exponential to first order in η and integrate over $\mathbf{r}$ to calculate the fluctuations in the observed flux. Substituting for η from (2.1), integrating by parts and normalizing to the mean flux, $\bar{F}$, we obtain the *fractional* intensity fluctuation

$$\delta F(\mathbf{x})\equiv\frac{\Delta F(\mathbf{x})}{\bar{F}}=\frac{4\mathcal{K}L}{\pi\sigma^6}\int d^2r\phi(r^2-\sigma^2)\exp\left(-\frac{r^2}{\sigma^2}\right), \tag{2.3}$$

with $\phi=\phi(\mathbf{x}+\mathbf{r})$. Throughout the paper, we use the symbol Δ to denote the fluctuation in some quantity and δ to describe its *fractional* fluctuation, as above.

BN calculate similar expressions for fractional fluctuations in the angular size of the image, Ω, the mean time delay of the pulse, t, and the pulse width, ϱ (the last two are normalized with respect to the mean pulse broadening $L\theta^2/2c$). Each of these quantities is of the form (*cf.* Appendix A)

$$\delta A_i(\mathbf{x},\mathcal{K})=\int d^2r\phi(\mathbf{x}+\mathbf{r},\mathcal{K})f_i(r,\mathcal{K}). \tag{2.4}$$

As the observer moves through the diffraction pattern at a speed **v**, these fluctuations will vary. The random internal velocities of the phase screen will generally be much smaller than **v**, and so a time lag T is equivalent to a spatial lag $\mathbf{s}=\mathbf{v}T$. The cross-correlations at lag **s** between the fluctuations in two quantities A_1 and A_2 is given by

$$\delta A_1(\mathbf{x}, \lambda_1)\,\delta A_2(\mathbf{x}+\mathbf{s}, \lambda_2)=\int d^2r_1\,d^2r_2\,\phi(\mathbf{x}+\mathbf{r}_1\lambda_1)\,\phi(\mathbf{x}+\mathbf{s}+\mathbf{r}_2, \lambda_2)f_1(r_1, \lambda_1)f_2(r_2, \lambda_2),$$

where f_1, f_2 denote any of the f_i. Taking two-dimensional Fourier transforms and averaging over all **x** keeping **s** constant gives the mean correlation (BN)

$$\langle\delta A_1(\mathbf{x}, \lambda_1)\,\delta A_2(\mathbf{x}+\mathbf{s}, \lambda_2)\rangle=\lambda_1\lambda_2\int\frac{d^2q}{(2\pi)^2}\,\tilde{f}_1(\mathbf{q},\lambda_1)\tilde{f}_2(\mathbf{q},\lambda_2)\,Q(\mathbf{q})\exp(i\mathbf{q}\cdot\mathbf{s}), \tag{2.5}$$

where

$$\tilde{f}_i(\mathbf{q},\lambda)=\int d^2r\,f_i(r,\lambda)\exp(-i\mathbf{q}\cdot\mathbf{r}) \tag{2.6}$$

$$Q(\mathbf{q})=\left\langle\frac{1}{\lambda_1}\,\tilde{\phi}(\mathbf{q}, \lambda_1)\,\frac{1}{\lambda_2}\tilde{\phi}^*(\mathbf{q},\lambda_2)\right\rangle/A \tag{2.7}$$

$$\tilde{\phi}(\mathbf{q},\lambda)=\int d^2r\,\phi(\mathbf{x}+\mathbf{r},\lambda)\exp(-i\mathbf{q}\cdot\mathbf{r}). \tag{2.8}$$

A random phase approximation has been used for $\tilde{\phi}(\mathbf{q})$. Since $\phi\propto\lambda$, $Q(q)$ is wavelength-independent and is given by the power spectrum of density fluctuations. The $\tilde{f}_i$ for the various parameters are listed in Appendix A. Each of these is of the form

$$\tilde{f}_i\propto P_i(q)\cos^{\alpha}(\psi)\exp(-\tfrac{1}{4}q^2\sigma^2), \tag{2.9}$$

where $P_i(q)$ is a polynomial in q and $\mathbf{q}\cdot\mathbf{s}=qs\cos(\psi)$. We compute the time averaged correlations (2.5) with $\lambda_1=\lambda_2$. For an isotropic power-law spectrum

$$Q(q)=Q_0q^{-\beta}, \tag{2.10}$$

the angular integrals in equation (2.5) generate Bessel functions and the wavenumber integrals give functions of the form

$$h_n^{\alpha}(s)\equiv\int_0^{\infty}(q\sigma)^{(2n+3-\beta)}\exp\left(\frac{-q^2\sigma^2}{2}\right)J_{\alpha}(sq)\,d(q\sigma)$$

$$=\left(\frac{s^2}{2\sigma^2}\right)^{\alpha/2}\frac{2^{(n+1-\beta/2)}}{\Gamma(\alpha+1)}\Gamma\left\{n+2+\frac{(\alpha-\beta)}{2}\right\}M\left\{n+2+\frac{(\alpha-\beta)}{2},\quad\alpha+1,\quad-\frac{s^2}{2\sigma^2}\right\} \tag{2.11}$$

where $M(a, b, x)$ is the confluent hypergeometric function (Abramowitz & Stegun 1970). The different angular factors of the Fourier transforms (2.9) will cause various combinations of the $h_n^i(s)$ to appear, so we define the following linear combinations, g_n^i:

$$g_n^2=\tfrac{1}{2}h_n^0-\tfrac{1}{2}h_n^2$$

$$g_n^4=\tfrac{3}{8}h_n^0-\tfrac{1}{2}h_n^2+\tfrac{1}{8}h_n^4 \tag{2.12}$$

and $g_n^0=h_n^0$. At zero lag ($s=0$) the g_n^i are proportional to h_n^0.

The mean auto- and cross-correlations of the fractional fluctuations are given by a dimensionless constant, K, characterizing the strength of the scattering medium, multiplied by some linear combination of the $g_n^{\alpha}(s)$. The auto-correlation of the flux fluctuations, for instance, is

$$\langle\delta F(\mathbf{x})\,\delta F(\mathbf{x}+\mathbf{s})\rangle=Kg_1^0(s), \tag{2.13}$$

where

$$K=\frac{Q_0\lambda^4L^2}{2\pi\sigma^{(6-\beta)}}\qquad\beta\leq4. \tag{2.14}$$

Similar expressions for other auto- and cross-correlations of interest are tabulated in Appendix A.

Correlations in wavelength can be derived by substituting the $\tilde{f}_i$ in equation (2.5) and evaluating with $\lambda_1 \neq \lambda_2$ and $s=0$. Several of the wavelength auto-correlations are also listed in Appendix A, where it is noted that the correlations are generally quite broad band.

The spot size on the screen, σ, can be calculated in terms of the assumed power spectrum, $Q_0 q^{-\beta}$. A simple order-of-magnitude estimate was given by BN who argued that the smallest scale phase fluctuation that scatters a ray is one that contributes a total phase change $\Delta\phi \gtrsim \pi$ (see also Gapper & Hewish 1981). The spectrum is thus truncated at an appropriate $q=q_{\max}$ and the mean square angular size of the image is estimated to be

$$\frac{\sigma^2}{L^2}=\lambda^4 \int_{q_{\min}}^{q_{\max}} \frac{d^2q}{(2\pi)^2} q^2 Q(q). \tag{2.15}$$

The integral is cut off below $q_{\min}=\sigma^{-1}$ because the corresponding spatial wavelengths are larger than σ and do not contribute to the image size. (For $\beta<4\lambda$, $q_{\min}$ can be taken to be 0.) In this paper, we use the following more exact evaluation of the angular size derived in Appendix B,

$$\sigma=L\lambda\left[\frac{\Gamma\{(6-\beta)/2\}\lambda^2 Q_0}{\pi(4-\beta)(\beta-2)\Gamma(\beta/2)}\right]^{1/(\beta-2)}. \tag{2.16}$$

Thus, given a power spectrum, one can solve (2.16) for σ and substitute into (2.14) to obtain the normalization of the fluctuation magnitudes.

We now consider the wander in the position of the image on the sky. If we take the vector $\mathbf{v}$ to denote the x direction, then the instantaneous angular displacement of the image along x from its 'true' time-averaged position is

$$\delta\theta_x \equiv \frac{\Delta\theta_x}{\sigma/L}=\frac{1}{\bar{F}}\frac{L}{\sigma}\int d^2r\, r_x I(\mathbf{r},\mathbf{x}), \tag{2.17}$$

where r_x is the distance from the point $\mathbf{x}$ on the phase screen in the x direction and $\Delta\theta_x$ is normalized by the image half-width, σ/L. Substitution from equation (2.1) and integration of equation (2.17) by parts gives

$$\delta\theta_x=\left(\frac{-2L\lambda}{\pi\sigma^7}\right)\int d^2r\,\phi(\mathbf{r}+\mathbf{x})\, r_x(3\sigma^2-2r^2)\exp(-r^2/\sigma^2). \tag{2.18}$$

There will also be fluctuations in the direction transverse to $\mathbf{v}$. This displacement $\delta\theta_y$ is obtained by substituting $_y$ for r_x in equation (2.18).

An examination of Fig. 1 reveals that one can expect some correlation between the angular displacement of the spot, θ_x, and the *rate of change* of the received flux. In particular, when the spot is shifted farthest from its mean position, the flux will be varying most rapidly. Further, there will be a similar correlation between F and the rate of change of θ_x. To compute $\dot{F}$ and $\dot{\theta}$ we take the derivatives of (2.3) and (2.18) with respect to $\mathbf{x}$ and normalize by the refractive time-scale $T_{\text{ref}} \sim \sigma/v$. Thus

$$\dot{F}\equiv\frac{\sigma}{\bar{F}}\frac{\partial F}{\partial x}=\frac{4L\lambda}{\pi\sigma^5}\int d^2r\frac{d\phi}{dr_x}(r^2-\sigma^2)\exp(-r^2/\sigma^2),$$

i.e.

$$f_{\dot{F}}=\frac{8L\lambda}{\pi\sigma^7} r_x(r^2-2\sigma^2)\exp(-r^2/\sigma^2). \tag{2.19}$$

Similarly, we write the normalized rate of wander of θ_x as

$$\dot{\theta}_x \equiv \sigma \frac{\partial \theta_x}{\partial x} = \frac{-2L\lambda}{\pi\sigma^2} \int d^2r \frac{d}{dr_x} [\phi r_x (3\sigma^2 - 2r^2) \exp(-r^2/\sigma^2)]$$

i.e.

$$f_{\dot{\theta}_x} = \frac{2L\lambda}{\pi\sigma^6} \{3\sigma^2 - 2r^2 - r_x^2(10 - 4r^2/\sigma^2)\} \exp(-r^2/\sigma^2). \tag{2.20}$$

Next we consider the expected elongation of the Gaussian image. If one averages over a time long compared to σ/v, the mean shape of a point source scatter-broadened by an *isotropic* ISM will be circular. However, since the fluctuations of the spot's diameter in two orthogonal directions are independent, the rms elongation of the scattering disc can be non-zero for an instantaneous 'snapshot' [i.e. a single realization of $\phi(\mathbf{r})$]. The spot will have some major axis with Gaussian width $2\sigma_1$ and a minor axis of width $2\sigma_2$. The orientation of these axes will be random, but we can relate σ_1, σ_2 to the measured widths along fixed axes x and y via the relations

$$\sigma_1^2 + \sigma_2^2 = 2\left(\int r_x^2 + \int r_y^2\right) = 2\int r^2 \tag{2.21}$$

$$\sigma_1^2 \sigma_2^2 = 4\left\{\int r_x^2 \cdot \int r_y^2 - \left(\int r_x r_y\right)^2\right\}, \tag{2.22}$$

where we have introduced the following notation for intensity-weighted averages

$$\int f(r_x, r_y) \equiv \int d^2r f(r_x, r_y) I(\mathbf{r}, \mathbf{x}).$$

Then, defining the elongation of the spot, e_s, as follows,

$$e_s \equiv \frac{\Delta\sigma}{\sigma} = \frac{\sigma_1 - \sigma_2}{\sigma} \simeq \frac{(\sigma_1^2 - \sigma_2^2)}{\sigma_1^2 + \sigma_2^2} \tag{2.23}$$

and substituting from (2.21) and (2.22), we have

$$e_s^2 = \left(\frac{\sigma_1^2 - \sigma_2^2}{\sigma_1^2 + \sigma_2^2}\right)^2 = \frac{\left\{\int (r_x^2 - r_y^2)\right\}^2 + \left(2\int r_x r_y\right)^2}{\left(\int r^2\right)^2}$$

$$= \frac{16L^2\lambda^2}{\pi^2\sigma^{16}} \left[\left\{\int d^2r \phi(\mathbf{x}, \mathbf{r}) r^2 (2\sigma^2 - r^2) \exp(-r^2/\sigma^2)\right\}^2 \right.$$

$$- 4\left\{\int d^2r \phi(\mathbf{x}, \mathbf{r}) r_x^2 (2\sigma^2 - r^2) \exp(-r^2/\sigma^2) \int d^2r \phi(\mathbf{x}, \mathbf{r}) r_y^2 (2\sigma^2 - r^2) \exp(-r^2/\sigma^2)\right\}$$

$$\left. + 4\left\{\int d^2r \phi(\mathbf{x}, \mathbf{r}) r_x r_y (2\sigma^2 - r^2) \exp(-r^2/\sigma^2)\right\}^2\right]. \tag{2.24}$$

3 Fluctuations in diffractive phenomena

The flux received from a typical pulsar is found to be correlated at any instant over both a frequency interval, the decorrelation bandwidth ν_{dc}, and a range of time lags, the scintillation timescale t_s. Moreover, when plotted as dynamic scintillation spectra in the frequency-time

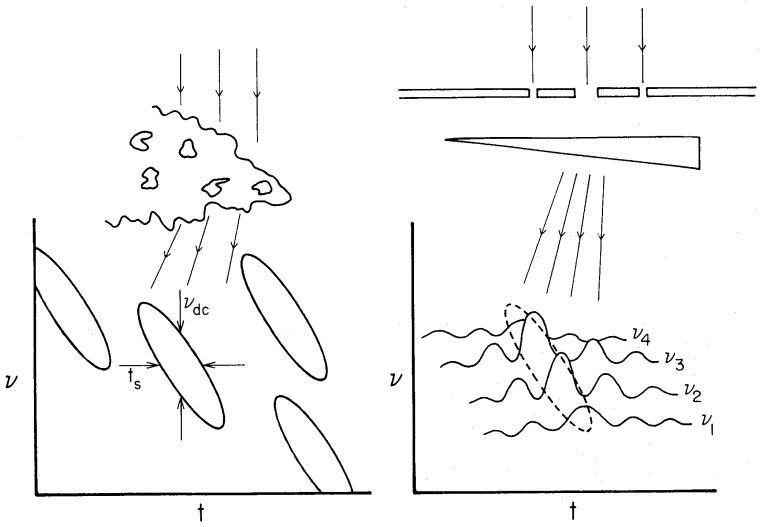

Figure 2. Refractive and diffractive contributions to the phenomenon of frequency drifts in dynamic scintillation spectra. For pulsars observed through the interstellar medium (left panel), the effect is produced by the combined action of small- and large-scale inhomogeneities. The scintillation time-scale t_s and the instantaneous decorrelation bandwidth ν_{dc} are indicated in the resulting frequency drift patterns. On the right we depict an equivalent optical system consisting of a diffracting mask and a dispersing prism. An observer moving past the pattern with velocity v detects intensity maxima at the different frequencies ν_4 to ν_1 ($\nu_4 > \nu_1$) at successively later times, leading to sloping bands in the frequency–time plane. In the example give, the diffracting mask has only a small number of slits, thus producing a *periodic* diffraction pattern as shown. Similar periodicities are sometimes seen in dynamic scintillation spectra of pulsars, suggesting that at these times the pulsar image is dominated by a few bright well-separated spots.

plane, the patterns of enhanced flux do not display uncorrelated modulation in the two coordinates but instead often show an organized drifting behaviour with a typical drift slope of order a few kHz s^{-1} (Fig. 2). These frequency drifts are believed to be caused by refractive density perturbations on large scales, $\gtrsim\sigma$, pictured either as large prisms (Shishov 1974; Hewish 1980) or as gradients causing the interference of a few distinct bundles of rays (Roberts & Ables 1982).

To include diffractive effects in our scattering model we must explicitly deal with the phases of the individual rays received by the observer. We conceptually decompose the image into a large number of point scatterers, each located at a position of 'stationary phase'. The mean separation of these scatterers on the screen is $a_{\min}$, giving $N\sim(\sigma/\alpha_{\min})^2$ scatterers. Since $N\gg1$ in the strong scattering limit, we may use statistical methods in the analysis of the interference of rays from these scattering centres. Consider a scatterer on the screen at a transverse distance r_j from the observer located at x. The phase advance of a wave propagating a distance L to Earth after being scattered at $\mathbf{r}_j$ consists of two parts: a free rotation over the distance propagated, $\theta_j=-(L+r_j^2/2L)/\lambda$, and an advance intrinsic to the phase screen, $\theta_j=\phi(\mathbf{x}+\mathbf{r}_j)\equiv\phi_j$. The *difference* in the total phase of a wave scattered from $\mathbf{r}_j$ on the phase screen, when the observer moves a distance Δx and changes his observation frequency to $\lambda+\Delta\lambda$, is given by

$$\Delta\theta_j=\frac{r_{xj}}{L\lambda}\Delta x+\frac{(L+r_{xj}^2/2L)}{\lambda^2}\Delta\lambda+\frac{\phi(\mathbf{x}+\mathbf{r}_j)}{\lambda}\Delta\lambda, \tag{3.1}$$

where we have taken the observer velocity to be in the x direction and have used the fact that $\Delta\phi=(\phi/\lambda)\Delta\lambda$. The electric vector received by the observer from the point j is described by $E_j\propto\exp(i\theta_j)$ and the total flux is $|\Sigma_j E_j|^2$. In the strong scintillation regime, we can assume that the θ_j are uniformly distributed and independent of one another. This is reasonable since the

scales that dominate diffractive scintillation are much smaller than σ. We then have $\langle \exp(i\theta_j)\rangle = 0$ and $\langle \exp\{i(\theta_j-\theta_k)\}\rangle = \delta_{jk}$, where θ_j, θ_k denote the phases of two electric vectors received at x, λ from two point $\mathbf{r}_j$, $\mathbf{r}_k$. Let $\theta_j+\Delta\theta_j$, $\theta_k+\Delta\theta_k$ denote the phases from the same points as seen at $x+\Delta x$, $\lambda+\Delta\lambda$, where $\Delta\theta_j$ is given by (3.1). The auto-correlation of the flux is then

$$\langle F(x,\lambda)\,F(x+\Delta x,\lambda+\Delta\lambda)\rangle = F^2\left\langle \frac{1}{N^2}\sum_{j,k,l,m}\exp\{i(\theta_j-\theta_k+\theta_l+\Delta\theta_l-\theta_m-\Delta\theta_m)\}\right\rangle \tag{3.2}$$

where for convenience we have assumed that the magnitudes of the electric vectors from the various scatters are the same. The $\Delta\theta_j$ of (3.1) have both a random part that is proportional to ϕ and a deterministic part. As we are only interested in the $1/e$ width of the flux correlation and not the details of its shape, it is reasonable to assume that the $\Delta\theta_j$ are distributed in a Gaussian manner. Then, summing (3.2) in pairs and using $\langle \exp\{i(\Delta\theta_j-\Delta\theta_k)\}\rangle = \exp\{-\langle(\Delta\theta_j-\Delta\theta_k)^2/2\rangle\}$, we can write the flux auto-correlation as

$$\langle F(x,\lambda)\,F(x+\Delta x,\lambda+\Delta\lambda)\rangle - F^2 = F^2\exp\{-\langle(\Delta\theta_j-\Delta\theta_k)^2\rangle/2\}. \tag{3.3}$$

When the relative phases from the various scatters within the image fluctuate by ~ 1 rad, the net intensity becomes decorrelated.

Thus, we need to estimate $\langle(\Delta\theta_j-\Delta\theta_k)^2\rangle$ as a function of Δx and $\Delta\lambda$ in a given realisation of the phase screen. Let $\mathbf{r}_1$, $\mathbf{r}_2$ denote the points of origin at the screen of two rays received at $\mathbf{x}$ and let $(\mathbf{r}_1-\mathbf{r}_2)\cdot\Delta\mathbf{x} = (x_1-x_2)\,\Delta x$. We now define via equation (3.1)

$$\begin{aligned} f(r_1,r_2) \equiv (\Delta\theta_1-\Delta\theta_2)^2 &= \left(\frac{x_1^2+x_2^2-2x_1x_2}{L^2\lambda^2}\right)(\Delta x)^2 \\ &+\left\{\frac{r_1^4+r_2^4-2r_1^2r_2^2}{4L^2\lambda^4}+\frac{\phi_1(r_1^2-r_2^2)+\phi_2(r_2^2-r_1^2)}{L\lambda^3}\right\}(\Delta\lambda)^2 \\ &+\left\{\frac{x_1(r_1^2-r_2^2)+x_2(r_2^2-r_1^2)}{L^2\lambda^3}+\frac{2\phi_1(x_1-x_2)+2\phi_2(x_2-x_1)}{L\lambda^2}\right\}\Delta x\,\Delta\lambda \end{aligned} \tag{3.4}$$

where, as before, we have kept terms to linear order in ϕ. The number density of scatterers within the image is clearly proportional to $I(\mathbf{r},\mathbf{x})$ defined in (2.2). Thus, to find the flux auto-correlation, (3.3), we must compute the intensity weighted average of $f(r_1, r_2)$ over all r_1, r_2 on the spot

$$\langle f(r_1,r_2)\rangle = \frac{\int d^2r_1\int d^2r_2\, I(\mathbf{r}_1,\mathbf{x})\,I(\mathbf{r}_2,\mathbf{x})\,f(r_1,r_2)}{\int d^2r_1\int d^2r_2\, I(\mathbf{r}_1,\mathbf{x})\,I(\mathbf{r}_2,\mathbf{x})}. \tag{3.5}$$

We evaluate the integrals to lowest order in ϕ and use the fact that f is symmetric with respect to r_1, r_2 to write (3.5) in the form

$$\begin{aligned} \langle f\rangle &= \langle(\Delta\theta_1-\Delta\theta_2)^2\rangle \equiv A(\Delta x)^2+B(\Delta\lambda)^2+C\Delta x\,\Delta\lambda \\ &= \left[\frac{\sigma^2}{L^2\lambda^2}-\frac{4}{\pi L\sigma^4\lambda}\int d^2r\,\phi\left\{2x^2\left(2-\frac{r^2}{\sigma^2}\right)-\sigma^2+r^2\right\}\exp(-r^2/\sigma^2)\right](\Delta x)^2 \\ &+\left\{\frac{\sigma^4}{2L^2\lambda^4}+\frac{2}{\pi L\sigma^2\lambda^3}\int d^2r\,\phi\left(\frac{r^6}{\sigma^4}-\frac{5r^4}{\sigma^2}+5r^2-\sigma^2\right)\exp(-r^2/\sigma^2)\right\}(\Delta\lambda)^2 \\ &+\left\{\frac{4}{\pi\sigma^2L\lambda^2}\int d^2r\,\phi x\left(4-\frac{7r^2}{\sigma^2}+\frac{2r^4}{\sigma^4}\right)\exp(-r^2/\sigma^2)\right\}\Delta x\,\Delta\lambda. \end{aligned} \tag{3.6}$$

From (3.3) we see that the auto-correlation of the intensity will fall to $1/e$ of its maximum value when $\langle f\rangle=2$. Let us define the scintillation time-scale t_s to correspond to the $1/e$ width along Δx of the flux auto-correlation. Thus, since t_s is the spatial coherence length of the diffraction pattern at Earth divided by the velocity $\mathbf{v}$, we have

$$t_s\equiv t_{s0}(1+\delta t_s)=\frac{\sqrt{2L\lambda}}{\sigma v}\left[1+\frac{2L\lambda}{\pi\sigma^6}\int d^2r\phi\{2x^2(2-r^2/\sigma^2)-\sigma^2+r^2\}\exp(-r^2/\sigma^2)\right] \tag{3.7}$$

where t_{s0} is the mean scintillation time-scale and δt_s is its fractional fluctuation. Similarly, the $1/e$ half width of the diffraction pattern in λ can be converted to units of frequency to find the instantaneous decorrelation bandwidth ν_{dc}

$$\nu_{dc}=\nu_{dc0}(1+\delta\nu_{dc})=\frac{Lc}{\pi\sigma^2}\left[1-\frac{2L\lambda}{\pi\sigma^{10}}\int d^2r\phi\{r^6-5r^4\sigma^2+5r^2\sigma^4-\sigma^6\}\exp(-r^2/\sigma^2)\right]. \tag{3.8}$$

Since the mean pulse broadening is described by the time constant $\tau_0=\sigma^2/2LC$ (*cf.* BN), we see that

$$2\pi\nu_{dc}\tau_0=1. \tag{3.9}$$

This 'uncertainty relation' has been verified observationally in the case of the Vela pulsar (Slee, Dulk & Otrupcek 1980). Furthermore, the fluctuation $\delta\nu_{dc}$ is the exact negative of the fractional fluctuation in the pulse broadening $\delta\tau$ [*cf.* (A.4) and (A.9)]. So we find that the uncertainty relation holds even for the fluctuations about the mean. This encourages us in believing that our simple scattering model can indeed be applied to diffractive phenomena.

The rotated ellipse described by (3.6) represents an 'average' frequency drift pattern for the given realization of the phase screen ϕ or, equivalently, the shape of the 2-*d* auto-correlation function in the (ν, t) plane. It is of interest to calculate the expected tilt or drift slope that an observer would measure. The angle of tilt will clearly depend on our scaling of the Δx and $\Delta\lambda$ axes; accordingly, we normalise by σ and λ, respectively. Then, taking ω to be the rotation from the orientation in the absence of refractive effects, we write the drift slope, m_d, as

$$m_d\equiv\tan\omega=\frac{\Delta x\lambda}{\Delta\lambda\sigma}=\left(\frac{d\nu}{dt}\cdot\frac{\sigma}{v\mathbf{v}}\right)^{-1}.$$

In terms of the coefficients A, B, C in (3.6)

$$m_d=\left(\frac{\sigma^2A-\lambda^2B}{\sigma\lambda C}\right)\left[-1+\left\{1+\left(\frac{\sigma\lambda C}{\sigma^2A-\lambda^2B}\right)^2\right\}^{1/2}\right]$$

$$\simeq\frac{4L\lambda}{\pi\sigma^5}\int d^2r\phi x(4-7r^2/\sigma^2+2r^4/\sigma^4)\exp(-r^2/\sigma^2). \tag{3.10}$$

The appearance of a dynamic scintillation spectrum is also characterized by the average elongation of its drift bands, e_d. This is a measure of the prominence of the frequency-drift phenomenon, since a circular pattern in the (ν, t) plane has no well-defined slope. As e_d again depends on the normalization chosen, we make an unambiguous definition by calculating the elongation at a fixed drift slope of $\pi/4$. Since observers tend to record the drift patterns with the most conspicuous drift, this will facilitate comparison with the data. We use a definition analogous to that used for e_s in Section 2. If the Gaussian drifting band has a semi-minor axis a and a semi-major axis b, then we define

$$e_d\simeq\frac{b^2-a^2}{b^2+a^2}. \tag{3.11}$$

We can eliminate a and b in favour of A, B and C to obtain

$$e_d = \frac{\{(A-B)^2+C^2\}^{1/2}}{A+B}.$$

Fixing the drift slope at $\pi/4$ with our normalization corresponds to setting $\sigma A = \chi B$ and letting C go to $C\cdot(\sigma A/\chi B)^{1/2}$. Thus, to first order in ϕ, we find that

$$e_d = 2^{3/2}\frac{L\chi}{\pi\sigma^5}\int d^2r\,\phi x\left(4-\frac{7r^2}{\sigma^2}+\frac{2r^4}{\sigma^4}\right)\exp(-r^2/\sigma^2). \tag{3.12}$$

4 Correlations

To compute the auto- and cross-correlations of the various quantities considered above, we take the Fourier transforms $\tilde{f}$ of the expressions for the fluctuations [(2.18), (2.19), etc.] and substitute into (2.5). These transforms, tabulated in Appendix A, can be grouped into two classes:

(I) Curvature-induced fluctuations (those $\tilde{f}$ that are real and proportional to even powers of q), i.e. δF, $\delta\Omega$, δt, $\delta\tau$, $\delta\nu_{dc}$, $\dot{\theta}$, δt_s;

(II) Gradient-induced fluctuations (those $\tilde{f}$ that are imaginary and proportional to odd powers of q), i.e. $\dot{F}$, $\delta\theta_x$, m_d, e_d.

In addition there are $\delta\theta_y$ and e_s^2 which do not belong to either class. Class I quantities correspond to those effects which are caused by focusing or defocusing *lenses*. Class II effects, on the other hand, are caused by *prisms* which steer the wavefronts. In general, one can expect Class I and

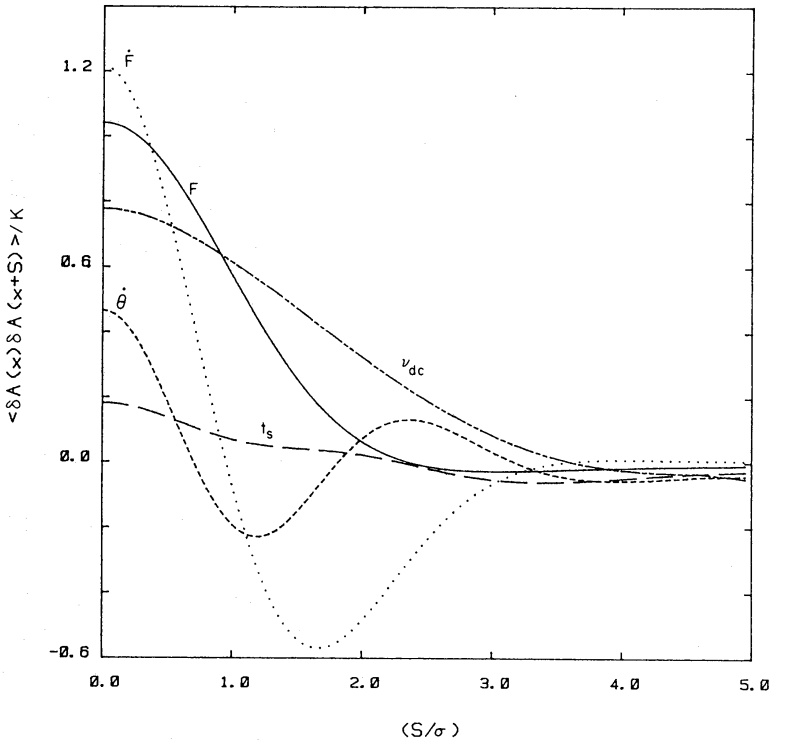

Figure 3. Normalized auto-correlations as a function of normalized spatial lag (s/σ), i.e. normalized time lag T/T_{ref} for a Kolmorogov spectrum ($\beta=11/3$). The flux F, its derivative $\dot{F}$, the rate of position wander $\dot{\theta}$, the decorrelation bandwidth ν_{dc} and the scintillation time-scale t_s are shown. The amplitudes are expressed in terms of the dimensionless constant K (equation 2.14) using the expressions given in Appendix A.

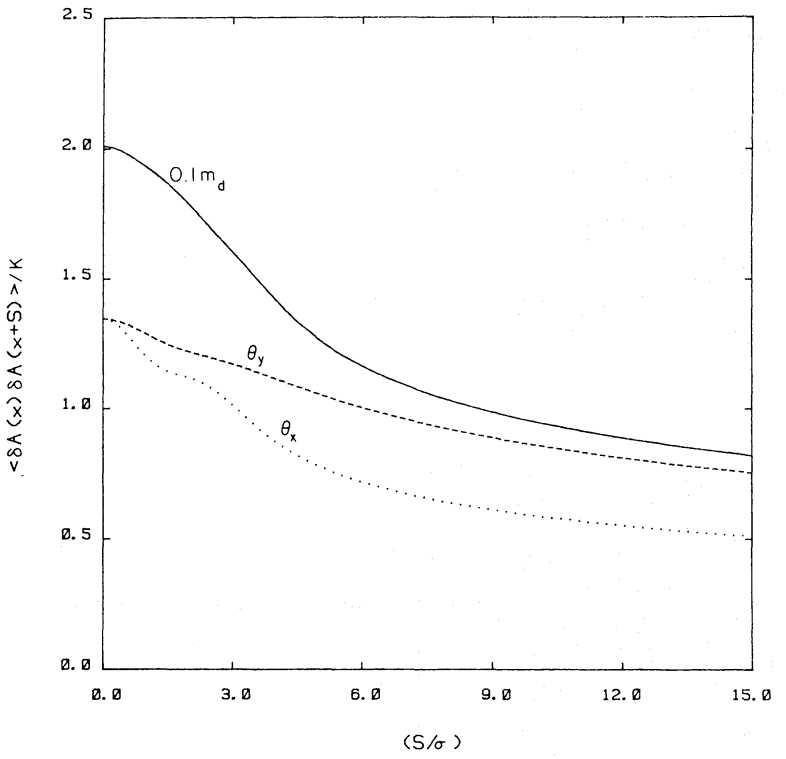

Figure 4. Normalized auto-correlations for $\beta=11/3$ of θ_x, the fluctuation in image position parallel to the direction of relative motion (dotted line), and θ_y (dashed line). The solid line corresponds to a tenth of the auto-correlation of the drift slope m_d. Amplitudes are in units of K and expressions are given in Appendix A. Note that the decorrelation time-scale of the fluctuations shown here is much greater than for those shown in Fig. 3. This is because θ_x, θ_y and m_d all have a divergent variance for $\beta \geq 4$ in the absence of an outer scale.

Class II quantities to co-vary among themselves, but not with each other. The strength of these cross-correlations is discussed in Section 7 and Table 2. The auto-correlations of the refractive fluctuations of the various observables that we have studied are shown in Figs 3 and 4 for a power-law spectrum with $\beta=11/3$ (expressions are given in Appendix A). We note that the variations with lag can be quite different from one another, although most of the curves have half-widths that are characteristically of order σ, as would be expected for a refractive effect. For a combined Earth-pulsar velocity of v this corresponds to the refractive time-scale

$$T_{\rm ref}=\frac{\sigma}{v}. \tag{4.1}$$

However, $\delta\theta_x$, $\delta\theta_y$ and m_d decorrelate over a time $\gtrsim 10\sigma/v$, a consequence of the incipient divergence in these quantities as $\beta \to 4$.

The Fourier transform of $f_{e_s^2}$ (A.8) has, as expected, no angular dependence. It is, in fact, identical to the square of $\tilde{f}_\Omega$, which means that the rms elongation of the spot is equal to the normalized rms fluctuation in the angular size. This is because the diameter fluctuations in orthogonal directions in the image are independent. Formally, e_s^2 will correlate with the parameters of group I, but as this is a higher-order effect, we do not calculate it. θ_y will be uncorrelated with any of the other quantities.

We also note that $\tilde{f}_{\dot{F}}\tilde{f}_{\theta_x}=-\tilde{f}_{\dot{\theta}_x}\tilde{f}_F$, so that the cross-correlations of these two pairs will be equal but opposite. This implies that, in the $(\delta F, \delta\theta_x)$ plane, a set of pulsar observations will statistically follow elliptical trajectories with a fixed sense of rotation (clockwise). Thus, an observer can gain a factor of $\sqrt{2}$ in the signal-to-noise ratio by measuring the *curl* of this field: $\Delta\theta\cdot\dot{F}-\dot{\theta}\cdot\Delta F$.

Certain other pairs of Fourier transforms are related, as well. We have already noted that $\tilde{f}_\tau = -\tilde{f}_{\nu_{dc}}$ and so the correlation functions of the latter follow immediately from those of the former. For frequency drifts, the rms elongation at fixed slope is seen to be half the rms value of the slope, m_d, so the average stretching of the drift slope bands is directly related to their inclinations. This is, however, a simple geometrical effect.

5 Density fluctuation spectra with $\beta > 4$

So far, we have considered spectra with $\beta \lesssim 4$ for which the arguments of Section 1 shows that the scattering is dominated by the small-scale density perturbations. Recent work (e.g. BN, GN, Hewish *et al.* 1985) has indicated that spectral indices greater than the critical value $\beta = 4$ may also be relevant to electron density perturbations in the ISM. In this regime, the scattering is dominated by the large spatial scales and, in the absence of an outer scale, the rms value of the bending angle $\eta(\mathbf{r})$ of (2.1) diverges. Accordingly, the linearization of the exponential in (2.2), which is central to the earlier development, is no longer valid. Most of the correlations computed in the previous section are nevertheless finite even for $\beta > 4$. This suggests that the divergence of $\eta(r)$ may be removable by a suitable modification of the theory.

For concreteness, we consider the variations in the flux, F. The auto-correlation function $C_{FF}(s)$ has a zero-lag magnitude $\sim K$ and has a half-width $s_{1/2} \sim \sigma$. This means that we are rarely interested in correlating observers separated by more than $\sim\sigma$. The mean bending angle seen by two such observers will be large but most of the bending is caused by large-scale perturbations ($q^{-1} \gg \sigma$) that contribute the same bending angle for both observers. This common steering will be indistinguishable from a shift in the image position. The physically interesting quantity, the *difference* in the bending between the two observers (equivalently the phase curvature or focusing of the screen) is, however, finite and reasonably small as shown below. Therefore we should obviously measure the bending angle with respect to some mean bending, η_0, common to the two observers. (We can take η_0 to be the refractive bending by the screen at a point half-way between the observers.) Equation (2.2) can now be written

$$I(\mathbf{r}, \mathbf{x}) = \frac{\bar{F}}{\pi\sigma^2} \exp\left[-\left\{\frac{L(\eta-\eta_0)+r}{\sigma}\right\}^2\right] \tag{5.1}$$

$$\simeq \frac{\bar{F}}{\pi\sigma^2}\left\{1 - \frac{2L\mathbf{r}\cdot(\eta-\eta_0)}{\sigma^2} + \varepsilon\right\} \exp(-r^2/\sigma^2)$$

where $\varepsilon \propto (\eta-\eta_0)^2 (L/\sigma)^2$. If we assume that ε is small compared to 1, we then have as before

$$\delta F = \frac{-2L}{\pi\sigma^4} \int d^2r \{\eta(\mathbf{r}+\mathbf{x}) - \eta_0\} \cdot \mathbf{r} \exp(-r^2/\sigma^2).$$

Since η_0 is a constant, terms proportional to it vanish by symmetry. Substituting (2.1) into this equation and integrating by parts, we recover (2.3) as before.

We must now show that ε in (5.1) can, in fact, be neglected. To do this we compute $\langle\{\eta(\mathbf{s}) - \eta_0\}^2\rangle$ for $s \sim \sigma/2$ (half the observer separation). From (2.1), (2.9) we have

$$\eta(\mathbf{s}) = \frac{-\lambda}{(2\pi)^2} \int d^2q (iq) \tilde{\phi}(q) \exp(iq\cdot s). \tag{5.2}$$

In computing $\langle\{\eta(\mathbf{s}) - \eta_0\}^2\rangle$, we should include only the effect of the refractive scales since the small scales $< \sigma$ have already been included in determining the spot size (Appendix B).

Equivalently, one notes that all the $\tilde{f}_i$ have a weighting factor $\exp(-q^2\sigma^2/2)$ which effectively damps out the small scales. We thus have

$$\frac{L_2}{\sigma^2}\langle\{\eta(s)-\eta(0)\}^2\rangle = 2K\left(\frac{s}{\sigma}\right)^{(\beta-4)}\int_0^\infty x^{3-\beta}\{1-J_0(x)\}\exp\{-x^2/2(s/\sigma)^2\}\,dx$$

$$= K2^{(4-b)/2}\Gamma\left(\frac{4-\beta}{2}\right)M\left(\frac{4-\beta}{2},\quad 1,\quad -\frac{s^2}{2\sigma^2}\right). \tag{5.3}$$

For $\beta>4$ we can evaluate (2.15) between $q=\sigma^{-1}$ and ∞ to obtain $K=\beta-4$. Substituting this in (5.3), we then find that (5.3) is small compared to 1 for $s\lesssim\sigma/2$ so long as $\beta\lesssim 5$. Since the range of β of interest to us is $3.5\lesssim\beta\lesssim 4.5$ (*cf.* GN), we are justified in neglecting ε in the expansion of (5.1). Similar arguments show that, for each of the other correlations computed above that remains finite for $\beta>4$ (i.e. $C_{\Omega\Omega}$, $C_{\Omega t_s}$, etc.), we may continue to use the expressions derived previously for $\beta<4$ as long as $s\lesssim\sigma$.

Certain correlations, however, are formally divergent for $\beta\leqq 4$. For example, the position shift, $\delta\theta$, depends directly on the bending angle and thus diverges at $\beta=4$. A steep spectrum (in the absence of some outer scale) will cause the image to wander arbitrarily far from its true position. Since an observer must estimate the true position by the mean over his observation period, $T_{\rm obs}=s/v$, the relevant measure of the amplitude of refractive position fluctuations is then the fluctuation across the duration of the observation, i.e.

$$\langle\{\delta\theta(s)-\delta\theta(0)\}^2\rangle = 2\langle C_{\theta\theta}(0)-C_{\theta\theta}(s)\rangle, \tag{5.4}$$

where $C_{\theta\theta}$ is the auto-correlation function of $\delta\theta$ (A.18). Although $C_{\theta\theta}$ diverges, the difference (5.4), equivalent to a first-order structure function in η, is finite for $\beta<6$. When $s\gg\sigma$, we can use (2.5) and (A.6) to obtain the following approximate estimate

$$\langle\{\delta\theta_x(s)-\delta\theta_x(0)\}^2\rangle \sim \frac{\lambda^4 L^2 Q_0}{2\pi\sigma^2}\int_{2\pi/s}^{1/\sigma} dq\, q^{3-\beta}$$

$$= K\ln(s/2\pi\sigma), \qquad \beta=4$$

$$= \frac{K}{(\beta-4)}\left(\frac{s}{2\pi\sigma}\right)^{\beta-4}, \qquad \beta>4. \tag{5.5}$$

Thus, when $\beta>4$, the image wander diverges in the limit of large baselines s. In practice, of course, the power-law spectrum (2.11) that we have considered will have a physical cut-off at some $q_{\rm min}$ and so the image wander will saturate for $s\gtrsim 2\pi/q_{\rm min}$.

The arrival time of pulses from a pulsar has a random delay whose dominant component is proportional to the mean phase fluctuations of ϕ averaged over the spot size σ on the scattering screen. This formally diverges for $\beta\geqq 2$. We note, however, that observers measure pulse arrival time residuals only after fitting a low-order polynomial model of intrinsic pulsar behaviour, $\Delta t=\alpha_1+\alpha_2 T+\alpha_3 T^2$, as well as sinusoidal components of period 1 yr to refine the position and proper motion of the pulsar. Consequentially, the *post-fit* arrival time residual $\Delta t_{\rm pf}$ is finite for all $\beta<8$. Blandford, Narayan & Romani (1984) have considered the effect of parameter-fitting on post-fit residuals. For the timing noise contributed by phase fluctuations in the ISM, we can apply their results in combination with (A.3) to obtain

$$\langle\delta t^2\rangle = \frac{4\lambda^4 L^2 Q_0}{2\pi\sigma^4}\int_0^\infty dq\, q^{1-\beta}\left(1-\frac{1}{2}q^2\sigma^2+\frac{1}{8}q^4\sigma^4\right)^2\exp\left(-\frac{1}{2}q^2\sigma^2\right)T(q), \tag{5.6}$$

where the transmission or filter function $T(q)$ is defined in the above-mentioned paper.

If the observations extend over a time $T_{obs} \gg 1$ yr and if $vT_{obs} \gg \sigma$, then we can use Table 1 of Blandford *et al.* (1984) to simplify (5.6) to

$$\langle \delta t^2 \rangle = \frac{4\lambda^4 L^2 Q_0}{2\pi\sigma^4} \int_{6.9/s}^{\infty} dq\, q^{1-\beta} = \frac{4K}{\beta-2}\left(\frac{s}{6.9\sigma}\right)^{\beta-2}, \qquad \beta \sim 4 \tag{5.7}$$

where the lower limit $q_{min} = 6.9/s$ in the integral is appropriate for $\beta \sim 4$ (i.e. spectral index ~ 3 in Blandford *et al.*). The divergences associated with arbitrarily large electron density perturbations are thus absorbed into the timing model. A similar treatment will excise the divergences in the cross-correlations of δt and other parameters.

The frequency drift slope dv/dt has, however, a divergence which *cannot be removed by the above techniques*. The drift slope is directly proportional to the phase gradient on the screen just as the position shift $\delta\theta$, but, unlike $\delta\theta$, the true mean value of dv/dt is known *a priori* to be 0. Thus, in the absence of an outer scale, a $\beta > 4$ spectrum will cause frequency drifts with arbitrarily large slope and this would be observed even in a single epoch of observations. Therefore, as discussed in Section 8, the finite observed drift slopes place limits on the perturbation.

6 Scattering by a thick screen

In the development so far we have assumed that the source is distant and that all the scattering is localized within a single thin screen at a distance L from the observer. In many circumstances (e.g. interplanetary scintillation) this will be a good approximation. It is, nevertheless, important to understand the changes that are introduced if the scattering is shared between several screens or indeed distributed uniformly along the line-of-sight to the source. Fortunately, the present formalism allows us to treat these cases as well.

Suppose that there are n phase screens between the source and the observer. Let the strength of the fluctuations on these screens be Q^i and the associated scattering angles be ϱ_i (equal to σ/L in the single-screen case). Denote the separation between screen i and screen j by L_{ij}, with $i=0$ signifying the source and $i=n+1$ the observer. The distant source case is recovered by taking the limit $L_{0i} \to \infty$.

Now consider a ray propagating from the source to the observer and undergoing angular deflections ξ_i at each of the n screens (Fig. 5). We can relate the transverse position vectors $\mathbf{r}_i$ of the intersections of the rays with the screens to the ξ_i through the recursion relation

$$\xi_i = \frac{\mathbf{r}_{i+1} - \mathbf{r}_i}{L_{ii+1}} - \frac{\mathbf{r}_i - \mathbf{r}_{i-1}}{L_{i-1i}}.$$

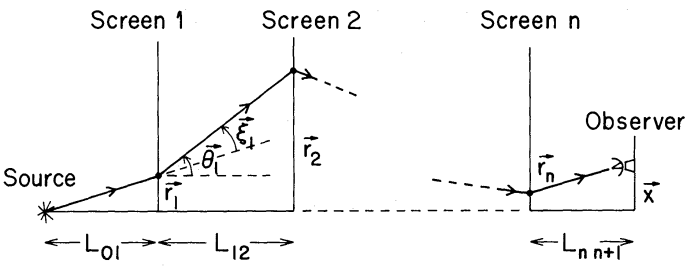

Figure 5. Scattering geometry for an extended medium represented by n thin screens. The angles θ_i and ξ_i described in the text are shown for screen 1 and a ray path that connects the source to the observer is denoted by the bold line.

We set $\mathbf{r}_0=0$ and denote the observer position by $\mathbf{r}_{n+1}=\mathbf{x}$ to obtain

$$\mathbf{r}_i=\frac{L_{0i}}{L_{0n+1}}\mathbf{x}-\sum_{j=1}^{n} M_{ij}\xi_j \tag{6.1}$$

where

$$M_{ij}=\begin{cases}\dfrac{L_{0j}L_{in+1}}{L_{0n+1}} & 1\leqq j\leqq i\leqq n\\[2ex] \dfrac{L_{0i}L_{jn+1}}{L_{0n+1}} & 1\leqq i\leqq j\leqq n\end{cases}. \tag{6.2}$$

The variables $\mathbf{r}_i$ and ξ_i are related by the Jacobian

$$\frac{\partial(\mathbf{r}_1,\mathbf{r}_2,\ldots,\mathbf{r}_n)}{\partial(\xi_1,\xi_2,\ldots,\xi_n)}=\left(\frac{L_{01}}{L_{0n+1}}\right)^2\prod_{i=1}^{n}L_{ii+1}^2. \tag{6.3}$$

Let $I_i(\mathbf{r}_i,\theta_i)$ be the intensity leaving the ith screen at an angle θ_i to reference direction. The intensity leaving the $(i+1)$th screen can then be written

$$I_{i+1}(\mathbf{r}_{i+1},\theta_{i+1})=\int\frac{d^2r_i}{L_{ii+1}^2}G_{i+1}\left\{\theta_{i+1}-\left(\frac{\mathbf{r}_{i+1}-\mathbf{r}_i}{L_{ii+1}}\right);\ \mathbf{r}_{i+1}\right\}I_i\left\{r_i,\left(\frac{\mathbf{r}_{i+1}-\mathbf{r}_i}{L_{ii+1}}\right)\right\} \tag{6.4}$$

where $G_i(\xi_i,\mathbf{r}_i)$ is the scattering kernel. Using the linear approximation outlined in Section 2, we write

$$G_i(\xi_i,\mathbf{r}_i)=\left(1+\chi\frac{\partial\phi_i}{\partial\mathbf{r}_i}\cdot\frac{\partial}{\partial\xi_i}\right)\frac{\exp(-\xi_i^2/\varrho_i^2)}{\pi\varrho_i^2}. \tag{6.5}$$

If the mean flux due to a point source as measured at the first screen is denoted by $\bar{F}_1$, the intensity at the observer plane can be written formally

$$I_n=\int\frac{d^2r_{n-1}}{L_{n-1n}^2}G_n\int\ldots\int\frac{d^2r_1}{L_{12}^2}G_2\cdot G_1\bar{F}_1 \tag{6.6}$$

where the integration must be carried out along a ray connecting the observer to the source.

Let us initially ignore refractive effects. The mean flux received by the observer is

$$\begin{aligned}\bar{F}\equiv\bar{F}_{n+1}&=\int\frac{d^2r_n}{L_{nn+1}^2}I_n\\&=\int\prod_{i=1}^{n}\left(\frac{d^2r_i}{\pi L_{ii+1}^2\varrho_i^2}\right)\bar{F}_1\exp\left(-\sum_{j=1}^{n}\xi_j^2/\varrho_j^2\right)=\bar{F}_1\left(\frac{L_{01}}{L_{0n+1}}\right)^2\end{aligned} \tag{6.7}$$

where we have incorporated the Jacobian from equation (6.3). This is just the inverse square law. Similarly, the mean angular size of the observed image is

$$\langle\theta^2\rangle=\frac{1}{\bar{F}}\int\frac{d^2r_n}{L_n^2{}_{n+1}}\theta_n^2I_n \tag{6.8}$$

where θ_n, the angle of the ray incident on the observer plane at $\mathbf{x}$, is given by

$$\theta_n=\frac{\mathbf{r}_1}{L_{01}}+\xi_1+\ldots+\xi_n-\frac{\mathbf{x}}{L_{0n+1}}=\sum_{i=1}^{n}\frac{L_{0i}}{L_{0n+1}}\xi_i. \tag{6.9}$$

So, using equations (6.3) and (6.7) we write the mean angular size of the image as

$$\langle\theta^2\rangle=\int\prod_{i=1}^{n}\left\{\frac{d^2\xi_i\exp(-\xi_i^2/\varrho_i^2)}{\pi\varrho_i^2}\right\}\cdot\left(\sum_{k=1}^{n}\frac{L_{0k}}{L_{0n+1}}\xi_k\right)^2=\sum_{i=1}^{n}\left(\frac{L_{0i}}{L_{0n+1}}\right)^2\varrho_i^2. \tag{6.10}$$

This is, as expected, the weighted sum of the individual scattering angular widths. Equation (6.10) agrees in the continuum limit with equation (A2) of BN.

Now we introduce refractive effects by including the phase fluctuations on the screens. The perturbation to the intensity can be written by combining equations (6.5) and (6.6) as

$$\delta I_n=\bar{\varkappa}\bar{F}_1\int\prod_{i=1}^{n-1}\left(\frac{d^2r_i}{\pi L_{ii+1}^2\varrho_i^2}\right)\sum_{j=1}^{n}\left(\frac{\partial\phi_j}{\partial\mathbf{r}_j}\cdot\frac{\partial}{\partial\xi_j}\right)\frac{\exp\left(-\sum_{k=1}^{n}\xi_k^2/\varrho_k^2\right)}{\pi\varrho_n^2}. \tag{6.11}$$

In the spirit of the earlier development, we express the phases ϕ_i as Fourier transforms and integrate by parts using equation (6.2) to obtain an expression for the normalized flux fluctuation

$$\begin{aligned}\delta F(x)&=\frac{1}{\bar{F}}\int\frac{d^2r_n}{L_{nn+1}^2}\delta I_n=\frac{\bar{\varkappa}\bar{F}_1}{\bar{F}}\int\prod_{i=1}^{n}\left\{\frac{d^2r_i\exp(-\xi_i^2/\varrho_i^2)}{\pi L_{ii+1}^2\varrho_i^2}\right\}\sum_{j=1}^{n}\left(M_{jj}\frac{\partial^2\phi_j}{\partial\mathbf{r}_j^2}\right)\\&=-\frac{\bar{\varkappa}\bar{F}_1}{\bar{F}}\int\prod_{i=1}^{n}\left\{\frac{d^2r_i\exp(-\xi_i^2/\varrho_i^2)}{\pi L_{ii+1}^2\varrho_i^2}\right\}\sum_{j=1}^{n}\int\frac{d^2q_j}{(2\pi)^2}\exp(i\mathbf{q}_j\cdot\mathbf{r}_j)\,M_{jj}q_j^2\tilde{\phi}_j.\end{aligned} \tag{6.12}$$

Equation (6.12) is the multi-screen generalization of equation (2.4). We obtain the generalization of the flux correlation function [equation (2.5) with $\varkappa_1=\varkappa_2$] by averaging over $\mathbf{x}$

$$\langle\delta F(\mathbf{x})\,\delta F(\mathbf{x}+\mathbf{s})\rangle=\varkappa^2\sum_{i=1}^{n}\int\frac{d^2q_i}{(2\pi)^2}\tilde{f}_F^i(\mathbf{q}_i)\tilde{f}_F^{i*}(\mathbf{q}_i)\,Q^i(\mathbf{q}_i)\exp\{i\mathbf{q}_i\cdot\mathbf{s}(L_{0i}/L_{0n1})\} \tag{6.13}$$

where

$$\tilde{f}_F^i(\mathbf{q}_i)=-\left(\frac{L_{0n+1}}{L_{01}}\right)^2\varkappa M_{ii}q_i^2\int\prod_{j=1}^{n}\left\{\frac{d^2r_j}{\pi L_{jj+1}^2\varrho_j^2}\exp(-\xi_j^2/\varrho_j^2-iM_{ij}q_i\cdot\xi_j)\right\}. \tag{6.14}$$

We can change from the variables $\mathbf{r}_j$ to the variables ξ_j using the Jacobian (6.3) and carry out the integrations to obtain

$$\tilde{f}_F^i(\mathbf{q}_i)=-\varkappa\,\frac{L_{0i}L_{in+1}}{L_{0n+1}}q_i^2\exp\left(-\frac{1}{4}q_i^2\sigma_i^2\right) \tag{6.15}$$

where σ_i, the effective size of the scattering disc at screen i, is defined by

$$\sigma_i^2=\sum_{j=1}^{n}M_{ij}^2\varrho_j^2. \tag{6.16}$$

If we have n evenly spaced similar screens and denote the distance from the source to the observer by D, then we can use equation (6.10) to obtain

$$\sigma_i^2=\frac{i(n+1-i)\{2i(n+1-i)+1\}D^2\langle\theta^2\rangle}{n(2n+1)(n+1)^2}. \tag{6.17}$$

Of greater interest is the continuum limit. We denote the distance along the line-of-sight

from the source by z and the mean scattering rate by $\psi(z)=\langle\Delta\varrho^2/\Delta z\rangle$. Then, letting $n\to\infty$, we obtain

$$\sigma^2(z)=\left(\frac{D-z}{D}\right)^2\int_0^z dz'\,z'^2\psi(z')+\frac{z^2}{D^2}\int_z^D dz'(D-z')^2\psi(z') \tag{6.18}$$

and

$$\langle\delta F(\mathbf{x})\,\delta F(\mathbf{x}+\mathbf{s})\rangle=\frac{\mathcal{K}^4}{D^2}\int_0^D dz(D-z)^2z^2\int\frac{d^2q}{(2\pi)^2}q^4\frac{dQ}{dz}\exp\left\{i\mathbf{q}\cdot\mathbf{s}\left(\frac{z}{D}\right)\right\}\exp(-q^2\sigma^2/2). \tag{6.19}$$

We have therefore expressed the auto-correlation function for the flux fluctuations as a sum (or an integral) over the scattering screens. To proceed further, we must substitute an expression for the spectrum of density fluctuations. For the spectrum in (2.10)

$$\frac{dQ}{dz}=q^{-\beta}\frac{dQ_0}{dz}. \tag{6.20}$$

Substituting in (6.13) the n-screen case gives

$$\langle\delta F(0)\,\delta F(s)\rangle=\frac{\mathcal{K}^4\Gamma(3-\beta/2)}{\pi 2^{(\beta/2-1)}}\sum_{i=1}^{n}\frac{M_{ii}^2Q_0^i}{\sigma_i^{6-\beta}}M\left\{\frac{6-\beta}{2},\quad 1,\frac{-s^2}{2(1-x)^2\sigma_i^2}\right\}, \tag{6.21}$$

while for a uniform medium we obtain

$$\langle\delta F(0)\,\delta F(s)\rangle=\frac{3K\Gamma(3-\beta/2)}{2^{2-\beta/2}}\int_0^1 dx\{x(1-x)\}^{\beta-4}M\left(\frac{6-\beta}{2},\quad 1,\quad\frac{-s^2}{2(1-x)^2\sigma_1^2}\right) \tag{6.22}$$

where K is given by the single-screen value (2.14) and σ_1 is $\theta_{\rm rms}D/2$ as for a single screen.

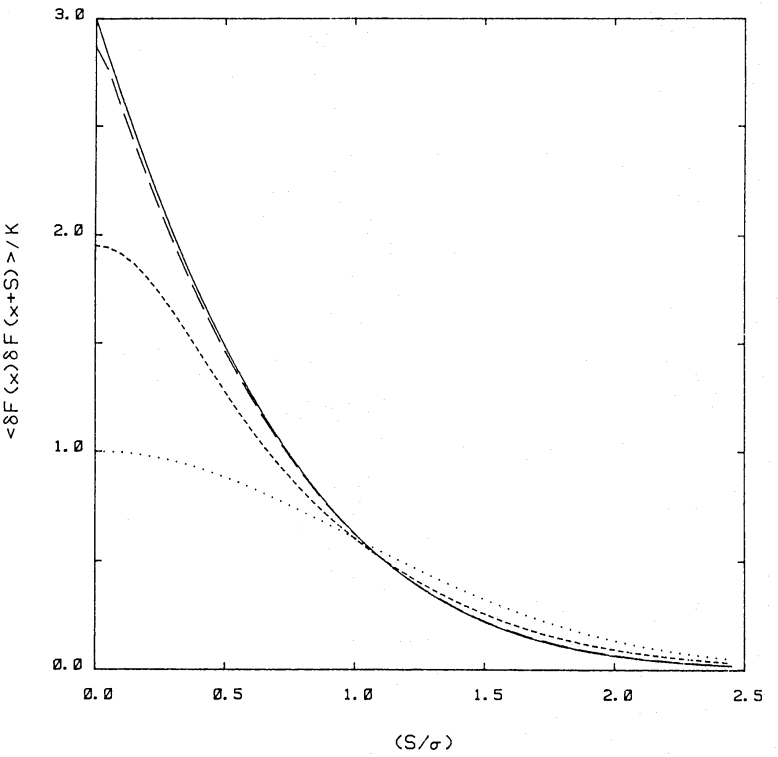

Figure 6. Normalized flux auto-correlation functions for a $\beta=4$ spectrum are shown for 1 (dots), 3 (short dashes), 5 (long dashes) equally spaced thin screens and for a continuous scattering medium (solid line). Normalization is in terms of the single-screen dimensionless constant K defined in equation (2.14).

In Fig. 6 we show the flux auto-correlation function for a uniform scattering medium with $\beta=4$ and compare this with the results for 1, 3, and 5 equally spaced screens. The single-screen case corresponds to the equivalent screen approximation introduced in BN and used in the earlier part of the present paper. We see that the rms refractive flux fluctuation at zero lag from a uniform medium is larger by a factor $\sqrt{3}$ than was predicted by the equivalent screen. In the case of a Kolmogorov spectrum (with $\beta=11/3$), the corresponding factor is 2.3, while for $\beta=4.3$ it is 1.4. For these three spectra the flux auto-correlation functions for an extended medium and single thin screen are shown in Fig. 7.

We have also calculated the angular size fluctuation auto-correlation and the cross-correlation with flux fluctuations. For a uniform medium with $\beta=4$ their expectation values at zero lag are 7/8 and 3/4, respectively, of the single-screen correlations.

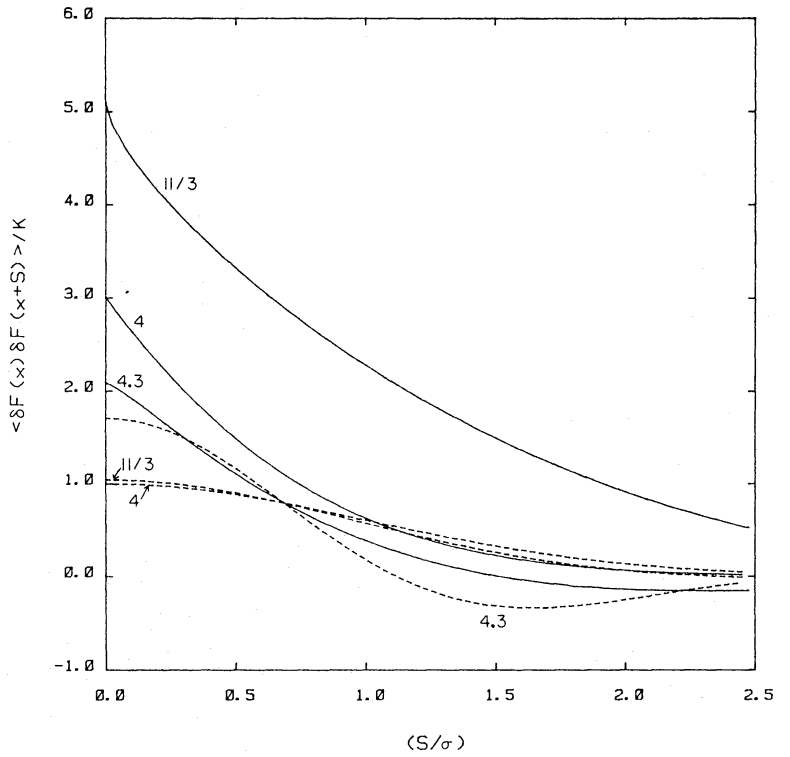

Figure 7. Comparison of the normalized flux auto-correlation functions for a single equivalent screen (dashed lines) and a continuous medium (solid lines) for three values of β(11/3, 4, 4.3). Normalization is in terms of the single-screen K in equation (2.14).

7 Numerical results

We now calculate the normalization, K, and numerical estimates of the fluctuations in various observables for three power-law models of the interstellar medim; $\beta=11/3$, $\beta=4$ and $\beta=4.3$. In the following we specialize to a *single-screen* equivalent to a uniform distribution of inhomogeneities between the source and the observer. (The theory of Section 6 for an extended medium could be used to obtain more accurate estimates, but the present status of the observations does not warrant such calculations.) For an extragalactic point source well out of the galactic plane one should replace $C_{-4}D$ by $3C_{-4}H\,csc(b)$ and D by $2H\,csc(b)$ in the expressions below and in Table 1, where b is the galactic latitude of the source and H is the scale height of the inhomogeneities in kpc (see Appendix A of BN for details).

We first assume that the power spectrum of phase fluctuations on the scattering screen has a Kolmogorov power-law form

$$Q(q)=Q_0 q^{-11/3}, \qquad Q_0=3.7\times10^{-18}C_{-4}D\ \mathrm{cm}^{-11/3} \tag{7.1}$$

which corresponds to $C_N^2=10^{-4}C_{-4}m^{-20/3}$ in the notation of Armstrong *et al.* (1981) (*cf.* BN). D is the distance to the pulsar measured in kpc. The amplitude Q_0 differs from that used by BN because they used an approximate estimate of the image angular size and needed to adjust Q_0 suitably to fit the observations. We avoid this by using the improved angular size estimate given in (2.16). The scaling of C_N^2 has been selected such that the parameter C_{-4} has a value ~1 for nearby pulsars. However, C_{-4} can be as large as $\sim10^4$ for distant pulsars in the plane of the galaxy and for the particular case of the Vela pulsar (Manchester & Taylor 1977; Cordes, Weisberg & Boriakoff 1984), and is $>10^5$ for the radio source at the galactic centre (Lo *et al.* 1985). We substitute (7.1) and (2.16) into equation (2.14) to obtain

$$K=1.27\times10^{-2}C_{-4}^{-2/5}\lambda^{-17/15}D^{-11/15} \tag{7.2}$$

where we measure the wavelength λ in metres.

We next consider the 'critical' spectrum with $\beta=4$. Here we fix the normalization constant Q_0 by requiring that the calculated angular size be the same as that for a Kolmogorov spectrum when $C_{-4}=\lambda=D=1$:

$$Q(q)=Q_0 q^{-4}, \qquad Q_0=1.6\times10^{-21}C_{-4}D\ \mathrm{cm}^{-4}. \tag{7.3}$$

Substituting in equations (2.14) and (2.15), where we retain the lower limit, we obtain

$$K=\frac{1}{\ln(430C_{-4}\lambda^3D^2/K^{1/2})}=\frac{1}{7\gamma} \tag{7.4}$$

where the correction factor γ is unity for $C_{-4}=\lambda=D=1$ and has only a weak logarithmic dependence on C_{-4}, λ and D.

Finally, we consider a spectrum with $\beta=4.3$. Rather surprisingly, the scalings of various observables with λ and D in this case are quite close to those with the Kolmogorov spectrum, so that a $\beta=4.3$ spectrum is equally compatible with scintillation observations as $\beta=11/3$ (GN). The refractive effects, however, will be much larger for $\beta=4.3$. For $\beta>4$, the lower cut-off at $q_{\min}\sim\sigma^{-1}$ will dominate the integral (2.15). Taking $q_{\max}=\infty$, we can solve for σ

$$\sigma=\left\{\frac{Q_0}{2\pi(\beta-4)}\right\}^{1/(6-\beta)}\lambda^{4/(6-\beta)}L^{2/(6-\beta)}. \tag{7.5}$$

If we again require that the calculated σ equal that for the Kolmogorov spectrum when $C_{-4}=\lambda=D=1$, we find that

$$Q(q)=Q_0 q^{-4.3}, \qquad Q_0=3.6\times10^{-25}C_{-4}D\ \mathrm{cm}^{-4.3}. \tag{7.6}$$

Substituting in (2.14) we find

$$K=(\beta-4)=0.3. \tag{7.7}$$

We use these three normalizations and the auto-correlation functions listed in Appendix A to calculate the magnitudes of the zero-order quantities and their rms fluctuations for the three spectra. These values, along with their scalings as a function of C_{-4}, λ, and D are listed in Table 1. As discussed in Section 5, certain quantities are formally divergent for large values of β. For these, we list approximate magnitudes of the fluctuations about the *observed* mean over the observation period as a function of that period in years, T_y.

The *normalized* cross-correlation of two parameters A and B is defined to be

$$C_{AB} = \frac{\langle AB \rangle}{\langle A^2 \rangle^{1/2} \langle B^2 \rangle^{2/2}}. \tag{7.8}$$

Class I (curvature-induced) fluctuations will correlate with one another to varying degrees, but will not be correlated with Class II (gradient-induced) fluctuations and vice-versa. We list the non-divergent Class I and II cross-correlations in Table 2.

8 Discussion

In the preceding sections, we have extended the computations of BN to include several more potentially observable effects arising from long-wavelength density fluctuations in the interstellar medium. We now have the theoretical machinery to estimate the magnitudes and time-scales of refractive effects for virtually any observable parameter in terms of any power-law spectrum of density fluctuations, including those with $\beta > 4$. We have also outlined the extension from a single screen to an extended medium and have shown how this can introduce significant changes.

Since the theory depends on a simple linearized model of the scattering (equation 2.2), we should address the question of the reliability of the theoretical predictions. Fortunately, Goodman & Narayan (1985) and references cited therein have presented exact results for the flux fluctuations produced by a single screen for both $\beta < 4$ and $\beta > 4$. A comparison between their results and those of our approximate theory is made in Appendix C. We find that the agreement is extremely good for $3.5 \lesssim \beta \lesssim 4.5$, encouraging us to believe that the other computed correlation functions are also quite accurate.

The detection of any of the fluctuations predicted by our theory, particularly the *cross-correlations*, would confirm the importance of propagation effects for the long time-scale variability of pulsars and compact extragalactic radio sources. The predicted magnitudes of the fluctuations are relatively small in the case of the Kolmogorov spectrum ($\beta = 11/3$), increasing with the observation frequency. On the other hand, if $\beta \geqq 4$, the fluctuations are relatively large but independent of λ. The shapes of the auto- and cross-correlations also depend on the value of β and upon whether the density fluctuations are restricted to a thin screen or are distributed throughout an extended scattering medium (see Fig. 7). Thus, observations of refractive effects promise to be a sensitive probe of the spectrum of ISM density perturbations as well as the distribution of the scattering irregularities along the line-of-sight.

Perhaps the easiest observations to make will be those that include fluctuations in the scintillation time-scale, δt_s, the decorrelation bandwidth, $\delta \nu_{dc}$, and the flux, δF. Since the fluctuation time-scale T_{ref} decreases as one moves to shorter wavelengths (Table 1), observations for a relatively short period at the highest frequency allowed by the multipath propagation condition, namely $\sigma > a_{min}$, should be sufficient to detect the predicted correlations. We note that the thin-screen theory predicts normalized cross-correlation coefficients of between 50 and 75 per cent (*cf.* Table 2), so the effects are large.

There are several possible VLBI experiments which could be carried out to detect refractive scintillation. Direct resolution of the scattered image of a pulsar would be most valuable. At meter wavelengths there are some candidates whose angular size fluctuations might just be detectable (*cf.* Bartel *et al.* 1984) but the time-scales involved will be rather long. Another possible VLBI experiment involves measuring the relative separation of pairs of pulsars close enough in the sky to be contained within the same primary beam of a radio telescope ($\sim 1°$), e.g. PSR 2016+28 and PSR 2020+28. This observation should be carried out at two or more low frequencies and it should be possible to achieve positional accuracies $\sim 0.1\lambda/b \sim 1$ milliarcsec.

The detection of a refraction-induced shift may be possible in the case of a steep spectrum of interstellar density fluctuations ($\beta \gtrsim 4$), though the variation time-scale will again be quite long. Some candidate pulsars are tabulated in BN.

Frequency drifts in dynamic scintillation spectra provide one of the best probes of large-scale density fluctuations (Hewish 1980; Roberts & Abkes 1982; Smith & Wright 1985; Hewish *et al.* 1985). The correlations of the drift slope with $\dot{F}$ and $\delta\theta$ are probably too small to be measured. However, the *magnitudes* of the drifts and their scaling with β, λ, D, and C_{-4} can be compared with our theory. Smith & Wright (1985) have measured the drift slopes of 32 pulsars. They present their data in the form

$$\frac{d\nu}{dt} = \frac{\nu v}{\theta_r D} \sec\phi, \tag{8.1}$$

where θ_r is the rms refractive bending angle and ϕ is the angle between the plane of maximum dispersion (i.e. the orientation of the ISM prism) and the pulsar velocity v. For 24 pulsars in which an independent measurement of v is available, they define $\theta_r = m\,\theta_s$ where θ_s is the rms scattering angle (i.e. σ/L), and estimate the value of $|m\cos(\phi)|$, a measure of the relative importance of long- and short-wavelength perturbations in the ISM. Noting that $\theta_s D = 2\sigma$, we can compute $|m\cos(\phi)|$ directly in our model, using the measured distances and scattering strengths for these 24 pulsars. For $\beta = 11/3$ we obtain $|m\cos(\phi)| = 0.40$, somewhat larger than the observed value of 0.24. Thus, the observed magnitude of refractive fluctuations in frequency drifts is *smaller* than that predicted by the Kolmogorov spectrum. On the contrary, the observed elongations of the drift patterns seem to be significantly larger than the value $e_d \lesssim 0.1$ expected for a Kolmogorov spectrum (although observational bias towards the most prominent examples may be reflected in the published spectra). Further, the mean observed flux variation is also larger than that predicted for a Kolmogorov spectrum (BN, GN). These conflicting indications might suggest that the continuous Kolmogorov power-law spectrum commonly assumed is too simplistic. They may also reflect deficiencies in the thin-screen model (*cf.* Blandford, Narayan & Romani 1985).

As further evidence that a single extended power-law spectrum with $\beta \lesssim 4$ is insufficient for the explanation of all scintillation phenomena, we consider the observation of periodicities in the spacing of the drift bands. Striking examples of quasi-periodic frequency drifts in dynamic scintillation spectra have been presented by Hewish *et al.* (1985). In these instances the patterns are interpreted as arising from the interference of a few, well-separated bundles of rays which have passed through an image-scale dispersive wedge on their way from the pulsar to the observer plane (*cf.* also Ewing *et al.* 1970; Roberts & Ables 1982). Hewish *et al.* go on to argue that the effective value of β can exceed 4. This attractive physical picture may, however, be difficult to realize in an extended power-law spectrum as the inhomogeneities intermediate between the diffractive scale and the spot size will generally break the image into too many beams to give the observed patterns. An alternative possibility is that the small-scale irregularities are absent and the spectrum has an inner scale somewhat smaller than the size of the image. This would create a few caustics which could give the observed periodic modulation. A consequence of this idea is that the periodicities of dynamic scintillation spectra should only be found at frequencies where the spot size is comparable to this inner scale and that this frequency should be larger for the more distant and more highly scattered pulsars.

Another implication of the observed quasi-periodicities is that a snapshot image of the pulsar would reveal a few bright blobs within the time-averaged spot (Fig. 2). GN have argued that such a 'fractal' geometry for the image is expected in theories with $\beta > 4$. This may be testable with VLBI on selected pulsars. The extended periodicities seen would probably still be rather rare unless the effective β were close to 6. However, a spectrum with $\beta > 4$ predicts extremely large values for the average drift slope (in fact, m_d will technically diverge) unless the spectrum cuts off

at lengths not much longer than the refractive scale σ. To maintain the large-amplitude refractive fluctuations indicated by other observations (e.g. flux), it might be necessary to impose an inner scale as well and invoke the focusing effects of caustics (*cf.* Section 1). (We note that there may already be evidence for caustics in the cusp-like peaks in pulsar intensity fluctuation records, e.g. Cole, Hesse & Page 1970; Helfand , Fowler & Kuhlman 1977.) The resulting spectrum of the ISM density perturbations would thus be severely truncated at both ends, containing only a limited power-law regime. GN showed that the λ and D scalings of observed quantities are relatively unaffected by the absence of short scales for $\beta>4$. If, however, $\beta<4$, then the absence of short-wavelength fluctuations drives the scaling laws towards the 'critical spectrum' case, i.e. $\beta=4$.

It is possible, for a given value of the spectral index β and a given distribution of the scattering inhomogeneities, to estimate an upper bound on the outer scale for the power-law spectrum from the observed angular broadening and the physical constraint that the amplitude of the electron density fluctations on this scale should be linear (i.e. $\delta n<n$). For spectra with $\beta\leqq 4$ the scattering is dominated by the smallest scale consistent with the strong scintillation condition, $a_{\min}\sim\lambda/\theta(a)$. To allow for the possibility that the spectrum cuts off at an inner scale somewhat larger than this, we define $a_{\min}\sim\alpha\lambda/\theta(a_{\min})$ with $\alpha\gtrsim 1$. If one has an independent estimate of the total number of scattering electrons, for example from the dispersion measure DM in the case of pulsars, one can use the scaling $\delta n(a)\propto a^{(\beta-3)/2}$ (Section 1) to estimate the scale at which the perturbation spectrum must become non-linear, i.e. $\delta n\sim n$. If we consider a source at distance z, a scattering screen of thickness L at z_0 and use the typical pulsar observables $\nu_{50}\equiv\nu_{\rm dc}$ (in units of 50 kHz) and DM_{30} (in units of 30 pc cm^{-3}), we find for a Kolmogorov spectrum

$$a_{nl}\simeq 4.2\times10^{20}\,\text{cm}\left[DM_{30}^{3}L^{-1.5}\left(\frac{z_0}{z}\right)^{1.75}\{\nu_{50}(z-z_0)\}^{1.25}\alpha^{-0.5}\lambda^{5.5}\right] \tag{8.2}$$

where λ is in metres and all other lengths are in kpc. This is an upper bound for the outer scale of the power-law spectrum. For spectra with $\beta>4$ the scattering is dominated by fluctuation scales on the order of the spot size $\sigma=\theta_{\rm rms}(z-z_0)$. We can again scale the fluctuation strength with the scale size to find an upper bound on the outer scale for a $\beta=4.3$ spectrum

$$a_{nl}\simeq 1.5\times10^{16}\,\text{cm}\left[DM_{30}^{1.54}L^{-0.77}\left\{\frac{z_0(z-z_0)}{z}\right\}^{0.88}\nu_{50}^{0.65}\lambda^{3.1}\right]. \tag{8.3}$$

If the application of this formula predicts in any particular pulsar that a_{nl} is less than the spot size σ, then refractive fluctuations cannot be important for that pulsar. For Vela and a few other pulsars, (8.3) is actually a significant constraint, as the bulk of the scattering is believed to be provided by the local effect of the Gum nebula. For Vela, $a_{nl}\sim\sigma$ when $\beta=4.3$, so refractive effects such as frequency drifts are likely to be quite restricted in such a steep spectrum.

Propagation-induced fluctuations can also be significant for sources other than pulsars. Rickett *et al.* (1984) suggested that the phenomenon of low-frequency variability of extragalactic radio sources can, in many cases, be explained as a propagation effect. The time-scales inferred from a spectrum of refractive fluctuations are compatible with those observed. Our theory predicts that the flux variations will be correlated with position shifts and angular size variations. Although the predicted magnitudes will be small, detection of this covariance using VLBI would allow a critical test of the ISM modulation hypothesis. There is the further possibility that the flicker of extragalactic radio sources (Heeschen 1984) could again be an effect of the ISM (Rickett *et al.* 1984; Simonetti, Cordes & Heeschen 1985; Blandford *et al.* 1985). In this context, it is worth noting that interstellar refraction by density irregularities should not affect the direction of linear polarization observed from pulsars and the compact components of extragalactic radio sources.

Observations by Lo *et al.* (1985) show that the VLBI resolved core of the galactic centre has a diameter ~ 2.1 *milliarcsec* at $\lambda = 1.35$ cm and that it scales with the observation wavelength as $\sim\lambda^2$, suggesting scatter-broadening. The source appears to be elongated at 3.6 cm with an axial ratio of 1.8:1, which corresponds to an elongation parameter $e_s \simeq 0.54$. From the source broadening we can estimate the scattering strength to be $C_{-4} \sim 5 \times 10^5$ (for $\beta = 4$). Using this value, we estimate the expectation value of e_s at $\lambda 3.6$ cm for an isotropic scattering medium to be $\lesssim 0.1$ unless β is somewhat greater than 4. We note, however, that observations of other sources near the galactic centre indicate significantly lower scatter-broadening. Hence, the bulk of the scattering medium is probably within ~ 100 pc of the galactic centre (Backer, private communication). Estimating the total number of electrons along the line-of-sight via the observed total extinction, one can use (8.2) to show that refractive effects in the galactic centre must be very small. As further confirmation for the unimportance of refractive effects for this source, we note that the data of Backer & Sramek (1982) place a limit of <10 milliarcsec on the wander of the source over a 5-yr baseline. Moreover, they find the centroids of the images at 3.6 and 11 cm to agree within 10 milliarcsec, indicating that there are no large-scale 'prisms' in the line-of-sight. A possibility one should consider is that the scattering medium in the vicinity of the galactic centre could be strongly anisotropic, as in the model by Higdon (1984), in which case the image spot would be elongated in the ratio of the scattering strengths along the two principal axes. For magnetic fields stretched in the plane of the Galaxy by differential rotation, the long axis of the image should be perpendicular to the galactic plane, as observed. A distinction between this picture and the random elongation we have considered (in Section 2) is that the position angle of the elongation will not change as a function of time for the anisotropic medium, whereas in our theory it is expected to do so on a time-scale $\sim T_{\rm ref} \sim \sigma/\mathbf{v}$. A second epoch of observations separated by $\gtrsim T_{\rm ref}$ would be helpful in clarifying this question.

In conclusion, we urge that future single-dish observations of radio pulsars include accurate measurements of the mean flux and the parameters τ, $\delta\nu_{\rm dc}$, δt_s, $m_{\rm d}$, and $e_{\rm d}$ which characterize the scintillation properties. In addition we advocate a modest simultaneous VLBI programme of observation of pulsars such as PSR 1818−04 designed to resolve the scatter-broadened image and detect position wander. Successful detections of the predicted correlations would, in addition to determining which variations in pulsars and extragalactic radio sources are intrinsic, also yield valuable data on the interstellar turbulence spectrum of particular relevance to theories of cosmic ray propagation. They would also motivate further calculations using the techniques outlined in this paper.

Acknowledgments

We thank J. Goodman for numerous discussions and D. Backer for advice on observations of the galactic centre. Support for this work was provided by the National Science Foundation under grant AST 84-15355. RWR is grateful to the Fannie and John Hertz Foundation for fellowship support.

References

Abramowitz, M. & Stegun, J. A., 1970. *Handbook of Mathematical Functions*, Dover Publications, New York.
Armstrong, J. W., Cordes, J. M. & Rickett, B. J., 1981. *Nature,* **291,** 561.
Backer, D. C. & Sramek, R. A., 1982. *Astrophys. J.,* **260,** 512.
Bartel, N., Cappallo, R. J., Ratner, M. I., Rogers, A. E. E., Shapiro, I. I. & Whitney, A. R., 1984. *VLBI and Compact Radio Sources,* p. 275, eds Fanti, R., Kellermann, K. & Setti, G., Reidel, Dordrecht, Holland.
Blandford, R. & Narayan, R., 1984. *Proceedings of the Workshop on Millisecond Pulsars,* eds Reynolds, S. P. & Stinebring, D. R., Green Bank, Va.

Blandford, R. & Narayan, R., 1985. *Mon. Not. R. astr. Soc.,* **213,** 591 (BN).
Blandford, R., Narayan, R. & Romani, R. W., 1984. *J. Astrophys. astr.,* **5,** 369.
Blandford, R., Narayan, R. & Romani, R. W., 1986. *Astrophys. J.,* **301,** L29.
Cole, T. W., Hesse, H. K. & Page, C. G., 1970. *Nature,* **225,** 712.
Cordes, J. M., Weisberg, J. & Boriakoff, V., 1984. *Astrophys. J.,* **288,** 221.
Ewing, M. S., Batchelor, R. A., Friefeld, R. D., Price, R. M. & Staelin, D. H., 1970. *Astrophys. J. Lett.,* **162,** L169.
Gapper, G. R. & Hewish, A., 1981. *Mon. Not. R. astr. Soc.,* **197,** 209.
Gochelashvily, K. S. & Shishov, V. I., 1975. *Opt. Quant. Electronics,* **7,** 524.
Goodman, J. & Narayan, R., 1985. *Mon. Not. R. astr. Soc.,* **214,** 519, (GN).
Heeschen, D. S., 1984. *Astr. J.,* **89,** 1111.
Helfand, D. J., Fowler, L. A. & Kuhlman, J. V., 1977. *Astr. J.,* **82,** 701.
Hewish, A., 1980. *Mon. Not. R. astr. Soc.,* **192,** 799.
Hewish, A., Wolszczan, A. & Graham, D. A., 1985. *Mon. Not. R. astr. Soc.,* **213,** 167.
Higdon, J. C., 1984. *Astrophys. J.,* **285,** 109.
Jakeman, E., 1982. *J. Opt. Soc. Am.,* **72,** 1034.
Jakeman, E. & Jefferson, H., 1984. *Optica Acta.,* **31,** 853.
Lee, L. C. & Jokipii, J. R., 1975. *Astrophys. J.,* **201,** 532.
Lo, K. Y., Backer, D. C., Ekers, R. D., Kellermann, K. I., Reid, M. & Moran, J. M., 1985. *Nature,* **315,** 124.
Manchester, R. N. & Taylor, J. H., 1977. *Pulsars,* Freeman, San Francisco.
Mutel, R. L., Broderick, J. J., Carr, T. D., Lynch, M., Desch, M., Warnock, W. W. & Klemperer, W. K., 1974. *Astrophys. J.,* **193,** 279.
Prokhorov, A. M., Bunkin, F. V., Gochelashvily, K. S. & Shishov, V. I., 1975. *Proc. IEEE,* **63,** 790.
Rickett, B. J., 1977. *Ann. Rev. astr. Astrophys.,* **15,** 479.
Rickett, B. J., Coles, W. A. & Bourgois, 1984. *Astr. Astrophys.,* **134,** 390.
Rino, C. L., 1979. *Radio Sci.,* **14,** 1147.
Roberts, J. A. & Ables, J. G., 1982. *Mon. Not. R. astr. Soc.,* **201,** 1119.
Rumsey, V. H., 1975. *Radio Sci.,* **10,** 107.
Salpeter, E. E., 1967. *Astrophys. J.,* **147,** 433.
Scheuer, P. A. G., 1968. *Nature,* **218,** 920.
Shapirovskaya, N. Ya, 1978. *Soviet astr.,* **22,** 544.
Shishov, V. I., 1974. *Soviet astr.,* **17,** 598.
Sieber, W., 1982. *Astr. Astrophys.,* **113,** 311.
Simonetti, J. H., Cordes, J. M. & Heeschen, D. S., 1985. *Astrophys. J.,* **296,** 46.
Slee, O. B., Dulk, G. A. & Otrupcek, R. E., 1980. *Proc. Aust. astr. Soc.,* **4**(1), 100.
Smith, F. G. & Wright, N. C., 1985. *Mon. Not. R. astr. Soc.,* **214,** 97.
Tatarskii, V. I. & Zavorotnyi, V. U., 1980. *Progress in Optics,* XVIII, p. 207, ed. Wolf, E.
Uscinski, B. J., 1977. *The Elements of Wave Propagation in Random Media,* McGraw-Hill, New York.

Appendix A:

The $\tilde{f}_i$ described by (2.7) are listed below for the various observables that we have considered, namely flux F, angular size Ω, pulse arrival time t, pulse width τ, time derivative of flux $\dot{F}$, position shift $\delta\theta_x$, time derivative of position shift $\dot{\theta}$, spot elongation e_s^2, decorrelation bandwidth ν_{dc}, scintillation time-scale t_s, drift slop m_d and elongation of drift pattern e_d.

$$\tilde{f}_F = -\frac{\varkappa L}{\sigma^2} q^2\sigma^2 \exp\left(-\frac{1}{4}q^2\sigma^2\right). \tag{A1}$$

$$\tilde{f}_\Omega = -\frac{\varkappa L}{\sigma^2}\left(q^2\sigma^2 - \frac{1}{4}q^4\sigma^4\right)\exp\left(-\frac{1}{4}q^2\sigma^2\right). \tag{A2}$$

$$\tilde{f}_t = 2\frac{\varkappa L}{\sigma^2}\left(1 - \frac{1}{2}q^2\sigma^2 + \frac{1}{8}q^4\sigma^4\right)\exp\left(-\frac{1}{4}q^2\sigma^2\right). \tag{A3}$$

$$\tilde{f}_r = -3/2\frac{\varkappa L}{\sigma^2}\left(q^2\sigma^2 - \frac{1}{3}q^4\sigma^4 + \frac{1}{48}q^6\sigma^6\right)\exp\left(-\frac{1}{4}q^2\sigma^2\right). \tag{A4}$$

$$\tilde{f}_{\dot{F}}=\frac{\varkappa L}{\sigma^2}(iq_x\sigma)q^2\sigma^2\exp\left(-\frac{1}{4}q^2\sigma^2\right). \tag{A5}$$

$$\tilde{f}_{\delta\theta x}=-\frac{\varkappa L}{\sigma^2}(iq_x\sigma)\left(1-\frac{1}{2}q^2\sigma^2\right)\exp\left(-\frac{1}{4}q^2\sigma^2\right). \tag{A6}$$

$$\tilde{f}_{\dot{\theta}}=-\frac{\varkappa L}{\sigma^2}(q_x^2\sigma^2)\left(1-\frac{1}{2}q^2\sigma^2\right)\exp\left(-\frac{1}{4}q^2\sigma^2\right). \tag{A7}$$

$$|\tilde{f}_{e_s^2}|^2=\frac{\varkappa^2L^2}{\sigma^4}\left(q^4\sigma^4-\frac{1}{2}q^6\sigma^6+\frac{1}{16}q^8\sigma^8\right)\exp\left(-\frac{1}{4}q^2\sigma^2\right). \tag{A8}$$

$$\tilde{f}_{\nu_{dc}}=3/2\ \frac{\varkappa L}{\sigma^2}\left(q^2\sigma^2-\frac{1}{3}q^4\sigma^4+\frac{1}{48}q^6\sigma^6\right)\exp\left(-\frac{1}{4}q^2\sigma^2\right). \tag{A9}$$

$$\tilde{f}_{t_s}=\frac{\varkappa L}{\sigma^2}\,q_x^2\sigma^2\left(1-\frac{1}{4}q^2\sigma^2\right)\exp\left(-\frac{1}{4}q^2\sigma^2\right). \tag{A10}$$

$$\tilde{f}_{m_d}=-4\ \frac{\varkappa L}{\sigma^2}(iq_x\sigma)\left(1-\frac{5}{8}q^2\sigma^2+\frac{1}{16}q^4\sigma^4\right)\exp\left(-\frac{1}{4}q^2\sigma^2\right). \tag{A11}$$

$$\tilde{f}_{e_d}=1/\sqrt{2}\tilde{f}_{m_d}=-2\sqrt{2}\ \frac{\varkappa L}{\sigma^2}(iq_x\sigma)\left(1-\frac{5}{8}q^2\sigma^2+\frac{1}{16}q^4\sigma^4\right)\exp\left(-\frac{1}{4}q^2\sigma^2\right). \tag{A12}$$

We substitute these expressions into (2.5) and evaluate according to (2.11) and (2.12) to obtain the various correlations. The auto-correlation functions are

$$\langle\delta F(\mathbf{x})\,\delta F(\mathbf{x}+\mathbf{s})\rangle=Kg_1^0. \tag{A13}$$

$$\langle\delta\Omega(\mathbf{x})\,\mathrm{d}\Omega(\mathbf{x}+\mathbf{s})\rangle=K\left(g_1^0-\frac{1}{2}g_2^0+\frac{1}{16}g_3^0\right). \tag{A14}$$

$$\langle\delta t(\mathbf{x})\,\delta t(\mathbf{x}+\mathbf{s})\rangle=K\left(g_{-1}^0-g_0^0+\frac{1}{2}-g_1^0\frac{1}{8}g_2^0+\frac{1}{64}g_3^0\right). \tag{A15}$$

$$\langle\delta\tau(\mathbf{x})\,\delta\tau(\mathbf{x}+\mathbf{s})\rangle=\frac{9}{4}K\left(g_1^0-\frac{2}{3}g_2^0+\frac{11}{72}g_3^0-\frac{1}{72}g_4^0+\frac{1}{2304}g_5^0\right). \tag{A16}$$

$$\langle\dot{F}(\mathbf{x})\,\dot{F}(\mathbf{x}+\mathbf{s})\rangle=Kg_2^2. \tag{A17}$$

$$\langle\delta\theta_x(\mathbf{x})\,\delta\theta_x(\mathbf{x}+\mathbf{s})\rangle=K\left(g_0^2-g_1^2+\frac{1}{4}g_2^2\right). \tag{A18}$$

$$\langle\delta\theta_y(\mathbf{x})\,\delta\theta_y(\mathbf{x}+\mathbf{s})\rangle=\frac{1}{2}K\left(h_0^0+h_0^2-h_1^0-h_1^2+\frac{1}{4}h_2^0+\frac{1}{4}h_2^2\right). \tag{A19}$$

$$\langle\dot{\theta}(\mathbf{x})\ \dot{\theta}(\mathbf{x}+\mathbf{s})\rangle=K\left(g_1^4-g_2^4+\frac{1}{4}g_3^4\right) \tag{A20}$$

$$\langle\delta(\nu_{dc})(\mathbf{x})\ \delta(\nu_{dc})(\mathbf{x}+\mathbf{s})\rangle=\frac{9}{4}K\left(g_1^0-\frac{2}{3}g_2^0+\frac{11}{72}g_3^0-\frac{1}{72}g_4^0+\frac{1}{2304}g_5^0\right) \tag{A21}$$

$$\langle\delta t_s(\mathbf{x})\ \delta t_s(\mathbf{x}+\mathbf{s})\rangle=K\left(g_1^4-\frac{1}{2}g_2^4+\frac{1}{16}g_3^4\right) \tag{A22}$$

$$\langle\delta\tan\omega(\mathbf{x})\ \delta\tan\omega(\mathbf{x}+\mathbf{s})\rangle=2\langle e_d(\mathbf{x})\ e_d(\mathbf{x}+\mathbf{s})\rangle$$

$$=16K\left(g_0^2-\frac{5}{4}g_1^2+\frac{33}{64}g_2^2-\frac{5}{64}g_3^2+\frac{1}{256}g_4^2\right). \tag{A23}$$

Equation (A15) diverges for $\beta \leqq 2$ and (A18), (A19) and (A23) for $\beta \geqq 4$. These are discussed in Section 5. The others are convergent for $\beta < 6$, but are reliable only for $\beta \lesssim 5$.

Auto-correlations with respect to changes in the observation frequency may also be of interest and we give these for certain parameters in (A24) to (A27). The frequency behaviour of position shifts are of interest since VLBI measurements can be performed at several frequencies. Fluctuations in ν_{dc} and t_s should also be accessible over a moderate frequency range.

$$\langle \delta\dot{F}(\lambda_1)\, \delta\dot{F}(\lambda_2)\rangle \propto \frac{\lambda_1^2\lambda_2^2\sigma_1\sigma_2}{(\sigma_1^2+\sigma_2^2)^{(8-\beta)/2}} \tag{A24}$$

$$\langle \delta\theta(\lambda_1)\, \delta\theta(\lambda_2)\rangle \propto \frac{\lambda_1^2\lambda_2^2}{\sigma_1^2\sigma_2^2}\,\frac{1}{(\sigma_1^2+\sigma_2^2)^{(4-\beta)/2}}\left\{\beta-3+(6-\beta)(4-\beta)\frac{\sigma_1^2\sigma_2^2}{(\sigma_1^2+\sigma_2^2)^2}\right\} \tag{A25}$$

$$\langle \delta\nu_{dc}(\lambda_1)\, \delta\nu_{dc}(\lambda_2)\rangle \propto \frac{\lambda_1^2\lambda_2^2}{(\sigma_1^2+\sigma_2^2)^{(6-\beta)/2}}\left[\frac{2\beta-9}{3}+\frac{(6-\beta)(8-\beta)}{6(\sigma_1^2+\sigma_2^2)^2}\left\{\frac{(\sigma_1^4+\sigma_2^4)}{2}+\frac{(\beta-2)}{3}\sigma_1^2\sigma_2^2\right.\right.$$
$$\left.\left.+\frac{1}{24}\,\frac{\sigma_1^4\sigma_2^4}{(\sigma_1^2+\sigma_2^2)^2}(10-\beta)(12-\beta)\right\}\right] \tag{A26}$$

$$\langle \delta t_s(\lambda_1)\, \delta t_s(\lambda_2)\rangle \propto \frac{\lambda_1^2\lambda_2^2}{(\sigma_1^2+\sigma_2^2)^{(6-\beta)/2}}\left\{2\beta-4+(8-\beta)(6-\beta)\frac{\sigma_1^2\sigma_2^2}{(\sigma_1^2+\sigma_2^2)^2}\right\} \tag{A27}$$

where $\sigma_{1,2}=\sigma(\lambda_{1,2})$ and $\sigma \propto \lambda^{\beta/(\beta-2)}$ for $\beta \leqq 24$ and $\sigma \propto \lambda^{4/(6-\beta)}$ for $\beta \geqq 4$. The constants of proportionality are given by the corresponding spatial auto-correlations evaluated at zero lag ($\mathbf{s}=0$). Numerically, we find that for $\beta=11/3$ the correlations reach their half-power points at the following values of λ_1/λ_2: $\dot{F}$, (0.6, 1.4); $\delta\theta$, (0.6, 1.8); ν_{dc}, (0.6, 1.4); t_s, (0.6, 1.4). For $\beta=4.3$ the half-power points are: $\dot{F}$, (0.7, 1.8); ν_{dc}, (0.6, 2.5); t_s, (0.6, 2.3). The fluctuation $\delta\theta$ grows arbitrarily large for $\beta > 4$. In general, the correlations are seen to be quite broad-band.

Normalized cross-correlations are given in Table 2.

Appendix B:

We wish to formalize the separation of the perturbation spectrum into diffractive and refractive regimes, leading respectively to angular broadening and refractive steering of the image of a point source. Let us imagine that we image the source with a Gaussian aperture of full-width W. We assume that W is intermediate between the diffractive scale, α_{min}, and the Fresnel scale, $r_F=\sqrt{\lambda L}$. (Note that, in the strong scintillation regime, $\alpha_{min} \ll r_F \ll \sigma$.) The angular amplitude of the signal received at the aperture is

$$\Phi(\alpha)=\frac{1}{\lambda}\int\int d^2x\, \exp\left(-i\frac{\alpha x}{\lambda}-\frac{2x^2}{W^2}\right)\mathbf{E}(x), \tag{B1}$$

where $\mathbf{E}(x)$ is the instantaneous electric vector measured at the point x on the observer plane. If we represent the source by a plane wave incident on the phase screen at a distance L and account for the phase rotations of the electric vectors received from different positions r on the phase screen, we can write this as

$$\Phi(\alpha) \propto \int\int d^2x d^2r\, \exp\left[-i\frac{\alpha x}{\lambda}-\frac{2x^2}{W^2}+i\left\{\phi(r)-\frac{(r-x)^2}{2L\lambda}\right\}\right]. \tag{B2}$$

Since $W \ll r_F$, we neglect the term in $x^2/L\lambda$. Integrating over x we then obtain

$$\Phi(\alpha) \propto \int d^2r \exp\left\{ i\phi(r) - \frac{-ir^2}{2L\lambda} - \frac{(r-\alpha L)^2 W^2}{8L^2\lambda^2} \right\}. \tag{B3}$$

We see that $\Phi(\alpha)$ is dominated by a region on the screen around the point $r=\alpha L$ of width $r_{tr} \sim \sqrt{8L\lambda}/W$. We now handle separately the phase fluctuations $\phi_<(r)$ due to scales smaller than r_{tr} and those $\phi_>(r)$ due to scales larger than r_{tr}. By Taylor expanding $\phi_>$ about $r=\alpha L$, we can write the argument of the exponent in (B3) as

$$\chi(r) = i\left\{ \phi_<(r) + \phi_>(\alpha L) + \phi_>'(\alpha L)(r-\alpha L) + \frac{1}{2}\phi_>''(\alpha L)(r-\alpha L)^2 - r^2/(2L\lambda) \right\} - \frac{W^2}{8L^2\lambda^2}(r-\alpha L)^2. \tag{B4}$$

The angular intensity is then given by

$$I(\alpha) = |\Phi(\alpha)|^2 \propto \int\int d^2r\, d^2r' \exp\{\chi(r) + \chi^*(r')\}.$$

We now introduce new coordinates $u = r + r' - 2\alpha L$, $v = r - r'$ and perform the integral over u. Since there are many diffractive scales $\alpha_{\min}$ within the range of integration, we can ensemble average over $\phi_<$. Thus

$$I(\alpha) \propto \int d^2v \exp\left\{ -\frac{1}{2} D_{\phi_<}(v) \right\} \exp\left\{ \frac{i}{\lambda}(\alpha - \lambda\phi_>')\, v \right\} \exp\left[-\left\{ \frac{W^2}{16L^2\lambda^2} + \frac{1}{W^2}(1 - \lambda L\phi_>'')^2 \right\} v^2 \right] \tag{B5}$$

where $D_{\phi_<}(v) \equiv \langle \{\phi_<(0) - \phi_<(v)\}^2 \rangle$ is the phase structure function at lag v due to scales smaller than r_{tr}.

Noting that the first exponential in (B5) cuts off at $v \sim \alpha_{\min}$, we now show that, over this range of v, the third exponential can be set to 1 with negligible error. For $W < r_F$, the first term in the argument of the third exponential is $\sim W^2 v^2 / r_F^4 < a_{\min}^2 / r_F^2 \ll 1$. Next, we have $v^2/W^2 \sim a_{\min}^2/W^2 \ll 1$, provided $W \gg \alpha_{\min}$ as already assumed. Finally, noting that $\alpha_{\min} \sim (\lambda^2 Q_0)^{-1/(\beta-2)}$ and $\phi_>''(r_{tr}) \sim \lambda^2 Q_0 r_{tr}^{\beta-6}$, we have

$$\frac{\lambda^2 L^2 \phi_>''^2 \alpha_{\min}^2}{W^2} \sim \left(\frac{\alpha_{\min} W}{r_F^2} \right)^{4-\beta} \ll 1$$

for the assumed range of W. Thus, (B5) simplifies to

$$I(\alpha) \propto \int d^2v \exp\left\{ 1 - \frac{1}{2} D_{\phi_<}(v) \right\} \exp\left\{ -\frac{i}{\lambda}(\alpha - \lambda\phi_>')\, v \right\}. \tag{B6}$$

Let us first neglect the contribution from $\phi_>'$ in the second exponential. $I(\alpha)$ is then given by the Fourier transform of $\exp\{-\frac{1}{2} D_{\phi_<}(v)\}$. Now, $D_{\phi_<}(v)$ varies as $v^{\beta-2}$ which, for $\beta \sim 4$, is not very different from v^2. We can therefore conveniently approximate $I(\alpha)$ by a Gaussian

$$I(\alpha) = \frac{\bar{F}}{\pi\theta_0^2} \exp\left(-\frac{\alpha^2}{\theta_0^2} \right), \tag{B7}$$

where the beam-width θ_0 can be determined in terms of the $1/e$ width of $\exp\{-\frac{1}{2} D_{\phi_<}(v)\}$ to be

$$\theta_0 = \lambda \left[\frac{\Gamma\{(6-\beta)/2\}\, \lambda^2 Q_0}{\pi(4-\beta)(\beta-2)\, \Gamma(\beta/2)} \right]^{1/(\beta-2)}. \tag{B8}$$

This leads to equation (2.16) for $\sigma=\theta_0 L$. When the contribution from $\phi'_>$ is included in (B6), the angular intensity received is modified to

$$I(\alpha)=\frac{\bar{F}}{\pi\theta_0^2}\exp\left[-\frac{\{\alpha-\lambda\phi'_>(\alpha L)\}^2}{\theta_0^2}\right] \tag{B9}$$

which is equivalent to equation (2.2).

Appendix C:

To test the accuracy of the approximations in our formalism, we compare our results with the exact results obtained by Goodman & Narayan (1985) for the flux fluctuations produced by a thin-scattering screen for power-law spectra with $2<\beta<6$. From (2.6) we see that the spectrum of the correlation $\langle\delta A_1(x)\,\delta A_2(x+s)\rangle$ is given by $\lambda^2\tilde{f}_1(q)\,\tilde{f}_2^*(q)\,Q(q)$. For flux fluctuations, we substitute from (A1) to obtain for a power-law spectrum of index β

$$\tilde{C}_{FF}(q)=Q_0\lambda^4L^2q^{4-\beta}\exp\left(-\frac{1}{2}q^2\sigma^2\right). \tag{C1}$$

In comparison, GN give for $\beta<4$,

$$\tilde{C}_{FF}(q)\equiv\tilde{W}(q)=Q_0\lambda^4L^2q^{4-\beta}\exp\left\{-\left(\frac{q}{q_{\rm ref}}\right)^{\beta-2}\right\}. \tag{C2}$$

We note that the normalization as well as the power-law index below the cut-off is identical. Moreover, the cut-off scales in the two formulae, namely $\sqrt{2}/\sigma$ and $q_{\rm ref}$, are also exactly equal, showing that our approximate theory is extremely accurate for $\beta<4$. The form of the cut-off is Gaussian in our theory because we have made the simplifying assumption of a Gaussian image whereas the exact result has the true spot shape. For $\beta\lesssim4$, however, the difference is small.

When $\beta>4$, our theory again predicts the form (C1) and GN still give

$$\tilde{C}_{\rm FF}(q)=Q_0\lambda^4L^2q^{4-\beta}, \qquad q<q_{\rm ref} \tag{C3}$$

so that the form and normalization of the spectrum below the cut-off continue to be in perfect agreement. However, whereas in (C1) we have a Gaussian cut-off at $q_{\rm ref}$, the true spectrum has a second power-law regime $\tilde{C}_{\rm FF}\propto q^{-4/(\beta-4)}$, $q_{\rm ref}<q<q_{\rm int}$ out to an intermediate scale $q_{\rm int}$. This region of the spectrum arises from the patchy 'fractal' nature of the image and is filtered out in our Gaussian approximation of the spot shape. Its contribution to the flux variance is, nevertheless, quite small. Thus the rms fluctuation of flux predicted by the present theory is

$$\delta F_{\rm rms}=\{Kh_1(0)\}^{1/2}=(\beta-4)^{1/2}2^{(2-\beta/2)}\,\Gamma(3-\beta/2), \tag{C4}$$

whereas the exact result given by Goodman & Narayan is

$$\delta F_{\rm rms}=\{2\sqrt{\beta-3}/(6-\beta)-1\}^{1/2}, \tag{C5}$$

This agrees with a similar result obtained by Jakeman & Jefferson (1984). A numerical comparison of (C4) and (C5) confirms that the agreement is quite good up to $\beta\sim4.5$.

We thus find that the approximate theory that we have developed is in very good agreement with more exact calculations in the regimes of interest. The advantage in our approach is that it can be extended to calculate a variety of effects that would be very difficult to compute using the more rigorous theory.